Hair follicle stem cell progeny heal blisters while pausing skin development

EMBOR-2020-50882V3.

Hair follicle stem cell progeny heal blisters while pausing skin development

Yu Fujimura[1], Mika Watanabe[1,2], Kota Ohno[3], Yasuaki Kobayashi[3], Shota Takashima[1], Hideki Nakamura[1], Hideyuki Kosumi[1], Yunan Wang[1], Yosuke Mai[1], Andrea Lauria[2,4], Valentina Proserpio[2,4], Hideyuki Ujiie[1], Hiroaki Iwata[1], Wataru Nishie[1], Masaharu Nagayama[3,5], Salvatore Oliviero[2,4], Giacomo Donati[2], Hiroshi Shimizu[1†], Ken Natsuga[1*]

[1]Department of Dermatology, Hokkaido University Graduate School of Medicine, Sapporo, Japan

[2]Department of Life Sciences and Systems Biology, Molecular Biotechnology Centre, University of Turin, Turin, Italy

[3]Research Institute for Electronic Science, Hokkaido University, Sapporo, Japan

[4]Italian Institute for Genomic Medicine, Candiolo (TO), Italy

[5]Japan Science and Technology Agency, CREST, Kawaguchi, Japan

[†]Deceased in February 2021

Conflicts of Interest

The authors declare that no conflicts of interest exist.

*Correspondence and reprint requests to:

Ken Natsuga, M.D., Ph.D.

Department of Dermatology, Hokkaido University Graduate School of Medicine

North 15 West 7, Sapporo 060-8638, Japan

Telephone: +81-11-716-1161, ext. 5962

E-mail: natsuga@med.hokudai.ac.jp

Abstract

Injury in adult tissue generally reactivates developmental programs to foster regeneration, but it is not known whether this paradigm applies to growing tissue. Here, by employing blisters, we show that epidermal wounds heal at the expense of skin development. The regenerated epidermis suppresses the expression of tissue morphogenesis genes accompanied by delayed hair follicle (HF) growth. Lineage tracing experiments, cell proliferation dynamics, and mathematical modeling reveal that the progeny of HF junctional zone stem cells, which undergo a morphological transformation, repair the blisters while not promoting HF development. In contrast, the contribution of interfollicular stem cell progeny to blister healing is small. These findings demonstrate that HF development can be sacrificed for the sake of epidermal wound regeneration. Our study elucidates the key cellular mechanism of wound healing in skin blistering diseases.

Keywords

Wnt signaling, epidermal stem cells, epidermolysis bullosa, basement membrane zone

Introduction

Tissue responds to injury by transforming its cellular components and extracellular matrix from homeostasis into a regenerative state. Damaged tissue typically reactivates an embryonic gene program in epithelia to accelerate tissue regeneration (Fernandez Vallone *et al*, 2016; Miao *et al*, 2019; Nusse *et al*, 2018; Yui *et al*, 2018). However, it is unknown whether this phenomenon also applies to injuries in developing tissue, in which the embryonic gene expression program is switched on before damage.

The epidermis is a stratified epithelium of the skin and is located on the surface of the body, where it serves as a barrier against external stimuli and microorganisms (Natsuga, 2014). Cellular proliferation and differentiation in the epidermal basal layer, where epidermal stem cells (SCs) are present, are fine-tuned to maintain the integrity of the epidermis (Donati & Watt, 2015). The epidermis attaches to the dermis through proteins in the epidermal basement membrane zone (BMZ) (McMillan *et al*, 2003). Epidermal BMZ proteins function as a niche for epidermal SCs (Watt & Fujiwara, 2011), and the loss of these proteins, such as α6 integrin (ITGA6), β1 integrin, and collagen XVII (COL17), leads to transient epidermal proliferation (Brakebusch *et al*, 2000; Niculescu *et al*, 2011; Watanabe *et al*, 2017).

Skin wounding causes pain and carries a significant risk of bacterial infection. The sources of skin wound healing have been extensively investigated in experimental animals (Dekoninck & Blanpain, 2019; Rognoni & Watt, 2018). Hair follicles (HFs), epidermal appendages, fibroblasts, and immune cells coordinate to heal the wound, and the contribution of each component can vary depending on the assay (Garcin *et al*,

2016). Wounding in adult skin induces the expression of genes regulating epidermal development, including SOX11 and SOX4 (Miao *et al.*, 2019).

Conventional skin wounding assays have employed full-thickness skin wounds, in which all skin components are removed, including the epidermis, epidermal appendages, dermis, and subcutaneous fat tissue. In contrast to conventional full-thickness skin wounds, epidermal detachment, as exemplified by subepidermal blisters, is distinctive because it does not affect the structures below the epidermis per se. The epidermis is detached from the dermis in several pathological conditions, such as burns (Chetty *et al*, 1992), congenital defects in epidermal BMZ proteins (epidermolysis bullosa (EB)) (Fine *et al*, 2014; Vahidnezhad *et al*, 2019), autoimmunity to these proteins (pemphigoid diseases) (Schmidt & Zillikens, 2013), and severe drug reactions, such as Stevens-Johnson syndrome/toxic epidermal necrolysis (White *et al*, 2018). Although the cells that contribute to the repair of full-thickness skin wounds have been identified (Aragona *et al*, 2017; Dekoninck & Blanpain, 2019; Donati *et al*, 2017; Gonzales & Fuchs, 2017; Ito *et al*, 2005; Kang *et al*, 2020; Page *et al*, 2013; Park *et al*, 2017; Sada *et al*, 2016), the cellular dynamics of subepidermal blister healing are completely unknown. In addition, full-thickness skin wounding, when applied to developmental skin, is unsuitable for distinguishing tissue regeneration and development. In contrast, blistering injury allows us to monitor both skin regeneration (reepithelization of the epidermis) and morphogenesis (HF development) within the same wound bed.

Here, by taking advantage of subepidermal blisters, we explore the effects of injury on developmental tissue. Unexpectedly, blistering injury is found to reduce the

expression of tissue morphogenesis genes in the healed epidermis and to direct HFSCs, rather than epidermal SCs, to provide progeny to heal the wound and to suspend HF development.

Results

Subepidermal blister formation and its healing process

The suction-blister technique was developed more than a half-century ago to selectively remove the epidermis from the dermis (Kiistala & Mustakallio, 1964, 1967), and it has been utilized to harvest epidermal pieces for transplant to repair human skin defects. We reasoned that suction blisters on neonatal mice, in which the epidermis is removed while HFs, the dermis, and subcutaneous fat tissues are maintained in the wounds, enable us to examine the direct relationship between tissue injury and skin development. Therefore, we applied constant negative pressure to the dorsal skin of C57BL/6 wild-type (WT) neonates to produce subepidermal blisters (postnatal day 1 (P1), **Figure 1A**). Histologically, skin separation occurred at the level of the dermoepidermal junction (DEJ) (**Figure 1B**, **Figure EV1A-C**). HFs, as shown by alkaline phosphatase (AP)-positive dermal papillae, remained on the dermal side of the blisters (**Figure 1B, Figure EV1D**). Dermis and subcutaneous tissues were intact after blistering (**Figure 1B**). α6 integrin (ITGA6), a hemidesmosome protein, was seen at the blister roof, whereas type IV collagen (COL4), a major component of the epidermal basement membrane, and laminin 332 (L332) were present at the base of the blister (**Figure 1C, Figure EV1B**). In line with the immunofluorescence data, hemidesmosomes localized on the blister roof and lamina densa (basement membrane) were observed at the blister base by electron microscopy (**Figure 1D**, **Figure EV1C**), as seen in human suction blisters (Kiistala & Mustakallio, 1967) and their murine counterparts (Krawczyk, 1971).

We then characterized the healing processes of the subepidermal blisters. One to two layers of the regenerated epidermis, marked with pan-cytokeratin, were found one

day after blister formation (P2, **Figure 1E**, **Figure EV1E**). The regenerated epidermis restored ITGA6 expression at the DEJ (**Figure 1E**, **Figure EV1E**). The shape of the basal keratinocytes in the intact skin was cuboidal or columnar (P2, keratin 14 (K14)-positive cells in the nonlesional area, **Figure 1F**). In contrast, the regenerated keratinocytes in the blistered skin transformed from cuboidal to a wedge/flattened shape (P2, K14-positive cells in the lesional area, **Figure 1F**) (Krawczyk, 1971). Two days after blistering (P3), the stratified epidermal layers were mostly restored but still lacked loricrin-positive granular layers, a hallmark of proper epidermal differentiation, in the lesional area (**Figure 1G**). The final step in epidermal differentiation was completed by the formation of loricrin-positive granular layers three days after blister formation (P4, **Figure 1H**). The immunofluorescence data for subepidermal healing are summarized in **Table EV1**. These results demonstrate that subepidermal blisters on neonates can serve a model for visualizing wound healing without damaging HFs and other dermal components at the developmental stage.

Epidermal restoration at the expense of skin development

To elucidate the effects of the blistering injury on the neonatal skin, we performed RNA-seq profiling of the wounded tissue above the dermis (the regenerated epidermis and the blister roof) one day after blistering (P2, **Figure 2A**, **EV2A**). Unexpectedly, the expression of genes involved in HF morphogenesis, such as Wnt signaling, melanogenesis, and Hedgehog signaling, was significantly downregulated (**Figure 2B, 2C, EV2B-D, Dataset EV1**). The HF undergoes morphogenesis in utero and after birth (**Figure EV1F**) (Paus *et al*, 1999; Saxena *et al*, 2019). In murine skin, HF

morphogenesis is classified into nine stages: the accumulation of nuclei in the epidermis without downward growth of HFs (stage 0), HFs with the most proximal part in the dermis (stages 1-5), and HFs with the most proximal part in the subcutaneous tissue (stages 6-8) (Paus *et al.*, 1999). The downregulation of HF morphogenesis genes (**Figure 2B, 2C**) led us to hypothesize that epidermal wounding tunes down tissue development to accelerate blister healing. In agreement with this hypothesis, the number of hair canals, which are tube-like connections between the epidermal surface and the most distal part of the inner root sheath (IRS) and are present in only developed HFs (HF morphogenesis, stage 6-8) (Paus *et al.*, 1999), was reduced in the regenerated epidermis (**Figure 2D, 2E**). HF growth under the regenerated epidermis at P4 was delayed at stages 5 and 6 where the IRS is halfway up to the HF or contains the hair shaft up to the level of the hair canal. In contrast, the surrounding intact skin of the blisters or the normal skin of the littermate controls had stage 7 HFs, in which the tip of the hair shaft leaves the IRS and enters the hair canal (**Figure 2F**). The observation of smaller HFs in the skin lesion when compared to the surrounding intact skin is accompanied by diminished Wnt signalling indicated by the LacZ-positive area in Wnt reporter mice (ins-Topgal+) (P2, **Figure 2G**).

The expression of genes involved in cytokine-cytokine receptor interactions and chemokine, TNF, IL-17, and JAK-STAT signaling pathways was increased in the regenerated epidermis (**Figure 2B, 2C, EV2B**), and these pathways are implicated in the recruitment of immune cells. However, the number of neutrophils, lymphocytes, and macrophages was not increased in the lesional dermis (P2, **Figure EV1G**), in which 1-2 layers of the regenerated epidermis covered the wound one day after blistering. There

was no apparent increase of these immune cells either at P4 (**Figure EV1G**), in which the whole epidermis was restored. These results suggest that the immune cells might not play a significant role in blister healing, although the involvement of immune cells or of molecules that they secrete—such as γδ T cell-derived Fgf9, which induces HF neogenesis (Gay *et al*, 2013)—cannot be fully excluded or may serve as a confounding factor affecting HF growth.

These data indicate that, in the context of skin morphogenesis where the immune system is not yet fully defined, subepidermal blisters heal at the expense of HF growth.

Progeny of junctional zone SCs represent the main cellular contribution to blister healing

Wounded lesions require epithelial cell proliferation and migration to restore skin integrity. We then investigated the dynamics of epidermal and HF keratinocytes during blister healing. One day after blister formation (P2), BrdU+ cells were abundant in the HFs and the intact epidermis adjacent to the blisters (**Figure 3A**). Cells positive for α5 integrin (ITGA5), a marker of migrating keratinocytes (Aragona *et al.*, 2017), were seen in the HFs within the lesional area and in the epidermal boundary between the blister and the nonlesional area (epidermal tongue) (**Figure 3B**, **Figure EV1E**). As HF growth was delayed in the regenerated epidermis (**Figure 2D-G**) and proliferative cells were abundant in HFs of the lesional area (**Figure 3A**), HF keratinocytes were deduced to participate in epidermal regeneration rather than in HF development.

To confirm this hypothesis, we employed a short-term lineage tracing strategy with suction blistering (**Figure 3C**). K14-lineage labeled cells (K14CreER:R26R-H2B-

mCherry or K14CreER:R26R-confetti), mainly progeny of SCs in the interfollicular epidermis (IFE), were sparse in the regenerated epidermis (**Figure 3D, 3E, Figure EV3A**). In contrast, most of the cells in the regenerated epidermis were Lrig1 (leucine-rich repeat and immunoglobulin-like domain protein 1)-lineage labeled cells (Lrig1CreER:R26R-H2B-mCherry or Lrig1CreER:R26R-confetti), which are the progeny of junctional zone SCs (**Figure 3F, 3G, Figure EV3A**). In line with this, phospho-Histone H3 (PH3)-positive cells were observed in Lrig1-lineage labeled cells at P2 (**Figure EV3B, 3C**). K14- and Lrig1-lineage labeled cells were increased from P1 (at the time of suction blistering) to P4 (sampling), but the expansion of Lrig1-lineage labeled cells was more evident in the regenerated epidermis (**Figure EV3D**). The expression of the Lrig1 gene was not upregulated in the regenerated epidermis at P2 in our RNA-seq. These data indicate that the HF junctional zone on the dermal side of the blister is the main pool for the keratinocytes that heal subepidermal blisters while halting HF development, although other hair follicle populations might also be involved in blister healing.

HF reduction from the wound bed of the blisters promotes the contribution of IFESC progeny to blister healing

The contribution of junctional zone HFSC progeny to blister healing led us to investigate how the epidermis regenerates in the absence of HFs at the blister base (dermis). Type XVII collagen (COL17) is expressed not only in the IFE but also in the bulge region of the HFs (**Figure 4A**) (Liu *et al*, 2019; Matsumura *et al*, 2016; Natsuga *et al*, 2019; Tanimura *et al*, 2011; Watanabe *et al.*, 2017). COL17 is encoded by the *COL17A1* gene,

and its deficiency leads to junctional EB (McGrath *et al*, 1995). The splitting of neonatal *Col17a1*$^{-/-}$ (Nishie *et al*, 2007) dorsal skin upon suction blistering was observed between ITGA6 and COL4/L332 (**Figure 4B, 4C**), as was the case in wild-type neonates (**Figure 1C, 1D**). Intriguingly, suction blistering (**Figure 1A**) of *Col17a1*$^{-/-}$ dorsal skin detached most, but not all, of the HFs from the dermis (P1, **Figure 4D**). In agreement with this finding, dermal papilla cells (AP+) were observed on the roof side of the blisters of *Col17a1*$^{-/-}$ mice, whereas the blister roofs of control mice did not have these cells (P1, **Figure 4E, Figure EV1D**). Epidermal regeneration was not apparent in *Col17a1*$^{-/-}$ mice one day after suction blistering (P2), whereas the control mice showed regeneration of the epithelial layers (**Figure 4F, Table EV1**). *Col17a1*$^{-/-}$ mice had delayed expression of loricrin in the regenerated epidermis three days after blister formation (P4, **Figure 4F, Table EV1**). BrdU+ cells were abundant in the *Col17a1*$^{-/-}$ mouse epidermis surrounding blisters as was the case for controls (**Figure 3A, 4G**). Lineage tracing experiments (**Figure 3C**) revealed that IFESC progeny covered most of the regenerated area (K14CreER:R26R-H2B-mCherry:*Col17a1*$^{-/-}$) at P4 (**Figure 4H, 4I**). The transgenic rescue of *Col17a1*$^{-/-}$ by overexpressing human COL17 (hCOL17+;*Col17a1*$^{-/-}$) (Nishie *et al.*, 2007) ameliorated blister healing (P4, **Appendix Figure S1, Table EV1**). These data demonstrate that upon detachment of most HFs from the dermis, the IFE can compensate the lack of junctional and HF SCs and repair defects in the IFE.

Impaired flattening of regenerated keratinocytes accompanies slower blister healing

We further sought to identify other modulators of subepidermal blister healing. We first focused on collagen VII (COL7), encoded by *Col7a1*. COL7 forms anchoring fibrils and is located at the DEJ (**Figure 5A**) but just below the basement membrane (Shimizu *et al*, 1997; Watanabe *et al*, 2018), and its deficiency leads to dystrophic EB (Christiano *et al*, 1993; Hilal *et al*, 1993). As conventional wound healing is delayed in COL7-hypomorphic mice (Nystrom *et al*, 2013), we applied the suction-blister method to *Col7a1*$^{-/-}$ mice (Heinonen *et al*, 1999) (**Figure 5B-H, Appendix Figure S2**). In contrast to that in WT and *Col17a1*$^{-/-}$ suction blisters (**Figure 1C, 1D, 4B, 4C**), skin splitting occurred at the level below the basement membrane in *Col7a1*$^{-/-}$ mouse dorsal skin, as shown by the presence of L332 and COL4 on the blister roof epidermis (P1, **Figure 5B, 5C**). The epidermal defects were not repaired in *Col7a1*$^{-/-}$ mice, whereas the epidermis of the control blistered skin regenerated one day after blistering (P2, **Figure 5F, Appendix Figure S2, Table EV1**), which is consistent with the delayed healing of full-thickness skin wounds in COL7-hypomorphic mice (Nystrom *et al.*, 2013). This finding is contrasted by the fact that COL7-depleted keratinocytes migrate faster than WT keratinocytes in vitro (Chen *et al*, 2002; Chen *et al*, 2000). We examined the HFs of *Col7a1*$^{-/-}$ mice to explain the slowed epidermal regeneration because HFs are the main contributor to blister healing (**Figure 3A-G**). However, HFs were present in the *Col7a1*$^{-/-}$ mouse wound bed (blister base) (P1, **Figure 5D, 5E**) as opposed to that of *Col17a1*$^{-/-}$ mouse (P1, **Figure 4D, 4E**). Moreover, the number of BrdU+ cells in HFs was comparable between *Col7a1*$^{-/-}$ and control mice (P2, **Figure 5G**, **Appendix Figure S2**), suggesting that the proliferation of HF keratinocytes does not account for the delayed blister healing of *Col7a1*$^{-/-}$ mice.

Second, we treated the blistered skin in wild-type mice with extracellular calcium (**Figure 5I-K**, **Appendix Figure S2**). Extracellular calcium is a potent inhibitor of proliferation and migration in cultured keratinocytes as well as an inducer of differentiation (Hennings *et al*, 1980; Magee *et al*, 1987). Consistent with previous in vitro assays, the intrablister administration of $CaCl_2$ (1.8 mM or 9.0 mM) just after suction blistering delayed epidermal regeneration in vivo (P2, **Figure 5I, Table EV1**). Premature differentiation, which might hinder wound healing, was not apparent in the $CaCl_2$-treated blisters, as K10 labeling was seen only at the blister roof but not in the keratinocytes on the wound bed (P2, **Figure 5I**). Similar to that in *Col7a1*$^{-/-}$ mouse blisters, the number of BrdU+ cells in HFs was not reduced in $CaCl_2$-treated blisters (P2, **Figure 5J**, **Appendix Figure 2**).

These two examples strongly suggest that there are factors other than HF keratinocyte proliferation that modulate blister healing. During blister healing, keratinocytes reshape into a wedge-shaped morphology (**Figure 1F**), which is mirrored by the RNA-seq data showing that the expression of genes involved in the regulation of the actin cytoskeleton is decreased in the regenerated epidermis (**Figure 2B, 2C**). Wedge-shaped/flattened keratinocytes are believed to be superior to cuboidal/columnar keratinocytes for covering epidermal defects. These data led us to wonder if the cell morphology was altered in settings of delayed blister healing. In the intact (nonblistered) skin, the morphology of *Col7a1*$^{-/-}$ or Ca-treated basal keratinocytes was similar to that of control cells (P2, the nonlesional area in **Figure 5F, 5H, 5I, 5K**). The regenerated keratinocytes became wedge-shaped/flattened in the control group, as shown in **Figure 1F**. However, the keratinocytes in the regenerated epidermis of *Col7a1*$^{-/-}$ or Ca-treated

mice were not as flat as those of control mice but were still rather cuboidal (P2, the lesional area in **Figure 5F, 5H, 5I, 5K**), which correlates with the delayed blister healing in these mice.

Mathematical modeling reproduces blister healing

These in vivo experiments led us to speculate that HF/IFE cell proliferation during paused HF development and the morphological changes of the regenerated keratinocytes might simply account for the dynamics of subepidermal blister healing. To answer this question, we employed mathematical modeling. We adopted an agent-based model (Kobayashi *et al*, 2016; Kobayashi *et al*, 2018), where keratinocytes were modeled by spheroids and cell division was described as replication of the spheroids. Such a model allowed us to visualize the dynamics of the epidermal basal layer and to establish the epidermal defects on the basement membrane. We utilized the data on the number of BrdU+ cells among HF vs. IFE keratinocytes (approximately 7:1 per unit of epidermal length; **Figure 3A**) and on the shape of the regenerated vs. normal keratinocytes (2:1 the length of the major cell axis; **Figure 5H, 5K**). SC progeny within the epidermal defects (colored in red), simulating HF-derived cells, had a more substantial contribution to wound healing than IFE SCs (colored in yellow; **Figure 6A, 6B, Movie EV1**), as seen in the lineage tracing experiments (**Figure 3C-G**). The absence of SCs within the epidermal defects, simulating HF reduction in the wound bed, showed delayed healing (**Figure 6C, 6D, Movie EV2**), in agreement with *Col17a1*$^{-/-}$ epidermal regeneration results (**Figure 4E-G**). A less flattened morphology of the regenerated keratinocytes, simulating *Col7a1*$^{-/-}$ and Ca-treated blister healing

(regenerated vs. normal keratinocytes, 1.3-1.6:1 in length; **Figure 5H, 5K**), slowed epidermal regeneration (**Figure 6E, 6F, Movie EV3**). By systematically changing the shape of regenerated vs. normal keratinocytes (from 1:1 to 2:1 in length) for different initial SC distributions within epidermal defects (**Figure EV4A**), we observed the same tendency: Less flattened morphology led to more delayed healing (**Figure EV4B, EV4C**), which suggests that the morphology affects healing dynamics irrespective of the initial SC distribution. These in silico data demonstrate that the contribution of HFSC progeny and the morphological change in the regenerated keratinocytes are sufficient to recapitulate the in vivo subepidermal blister healing.

We finally asked whether this HF contribution to wound healing could be applied to a human setting, in which HFs are larger but much more sparsely distributed than their murine counterparts (**Table EV2**). We examined human subepidermal blister samples and found that epidermal regeneration by HFs was observed in the samples with the re-epithelized area (**Figure EV5**). These findings from human samples are consistent with the mice data.

Discussion

Although recent studies have reported that injury causes damaged tissue to shift to an embryonic-like state, there is a poor understanding of how regeneration affects development at the damaged tissues. Here, we applied the blistering injury to neonatal mouse dorsal skin and showed the skewed contribution of HFSC progeny to wound healing rather than HF development.

Previous studies on skin wounding combined with the fate mapping of murine skin delineated the involvement of epithelial, mesenchymal, and immune cells in wound healing, depending on different settings (Dekoninck & Blanpain, 2019; Rognoni & Watt, 2018). However, as full-thickness skin wounds, even when they are applied to neonatal skin, remove all skin components, it is challenging to see the effects of development on injury or vice versa. Our blistering injury has an advantage over conventional skin wounding studies in that only the epidermis is removed by constant negative pressure, with the other skin components and basement membrane being retained in the wounds, which allowed us to examine “pure” epidermal wound healing processes during skin development. Our study contrasts with wound-induced embryonic gene expression (Miao *et al.*, 2019) and follicular neogenesis upon full-thickness skin wounding in adult (Ito *et al*, 2007; Osaka *et al*, 2007) and neonatal mice (Rognoni *et al*, 2016). So far, our study has not distinguished whether the waning Wnt signaling was the primary cause, or the result, of the delayed HF morphogenesis. Further studies are needed to clarify this.

Previous studies have suggested the possible involvement of HFs in epidermal regeneration in human suction blisters (Lane *et al*, 1991) and extracellular matrix

alterations in the skin-split area (Hertle *et al*, 1992; Leivo *et al*, 2000). We show that the progeny of HF junctional zone SCs mainly repair subepidermal blisters (**Figure 3F, 3G, 6A, 6B**), although the involvement of other HF populations cannot be excluded. However, the IFE can also serve as a reservoir of keratinocytes to repair epidermal defects when most HFs are detached from the dermis (**Figure 4H**). How the contribution of two sources of keratinocytes to blister healing is regulated is unknown, but the significant contribution of HF junctional zone progeny is reasonable because HFs are densely located in the wound bed (blister base). In contrast, the progeny of IFESCs could recover only from the blister edge, as demonstrated by mathematical modeling (**Figure 3D-3G, 6A, 6B**). The role of HFSCs is also highlighted by delayed HF growth in the regenerated epidermis, as corroborated by the downregulated Wnt signaling (**Figure 2A-2G**). These findings indicate that there is a coordinated balance between tissue development and wound healing, which has not been well recognized. In addition, the expression of IL-17 signaling pathway genes was increased, although the recruitment of immune cells was not evident one day or three days after blistering (**Figure EV1G**). Recently, IL-17 signaling has been shown to drive Lrig1-lineage cell recruitment in wound healing and tumorigenesis (Chen *et al*, 2019). Therefore, IL-17 signaling might also help Lrig1-lineage cells translocate from HFs to repair epidermal defects in our study (**Figure 3F, 3G**).

The dynamics of cytoskeletal changes directly affect cellular morphology and migration potential (Tang & Gerlach, 2017). Previous studies have shown that cells undergo a morphological transformation into a wedge/flattened shape at the leading edge of migrating cells (Uroz *et al*, 2019) and in regenerated keratinocytes during

wound healing (Krawczyk, 1971; Paladini *et al*, 1996). Our study has shed further light on the significant impact of the keratinocyte morphological changes on in vivo wound healing through blistering experiments in *Col7a1*$^{-/-}$ and Ca-treated mice and mathematical modeling (**Figure 5F, 5H, 5I, 5K, 6A, 6E, 6F**). However, the morphological changes of keratinocytes might not directly foster blister healing but might be simply correlated with other primary causes that help regenerate the epidermis. The loss of a functional basement membrane in the *Col7a1*$^{-/-}$ blister bottom might slow blister healing due to the lack of substrates for cell migration. Pressure during blister induction could be a factor that changes the cellular morphology. Additional mechanistic studies are needed to verify the hypothesis we raise in our study.

Our in vivo blistering experiments can mimic and replace the in vitro cultured cell wound healing assay (e.g., scratch wounding), which has been used in the field of cell biology for decades because subepidermal blisters are epidermal wounds. In vivo intrablister administration of drugs, as exemplified by extracellular calcium administration (**Figure 5I**), could be an alternative to in vitro chemical treatment of scratch-wounded cultured cells to develop new therapeutic options for wound healing, especially of subepidermal blisters.

Our in vivo suction-blister model recapitulates the human pathological epidermal detachment seen in EB, pemphigoid diseases, burns, and severe drug reactions such as Stevens-Johnson syndrome/toxic epidermal necrolysis. Loss-of-function mutations in *COL17A1* (McGrath *et al.*, 1995) and *COL7A1* (Christiano *et al.*, 1993; Hilal *et al.*, 1993) lead to junctional and recessive dystrophic EB in humans, respectively. Therefore, *Col17a1*$^{-/-}$ and *Col7a1*$^{-/-}$ mouse blistering also serves as an EB wound model. The

prominent hair loss in human *COL17A1*-mutated junctional EB might be reflected by the reduction of HFs from the wound bed in *Col17a1*$^{-/-}$ blisters (**Figure 4D, 4E**), whereas the hair loss in recessive dystrophic EB is not as severe as that in the junctional subtype (Tosti *et al*, 2010), consistent with the maintenance of HFs in the dermis of *Col7a1*$^{-/-}$ mouse dorsal skin upon suction blistering (**Figure 5D, 5E**). It is plausible that recurrent blistering can exhaust the pool of HFSCs, leading to delayed blister healing and scarring, especially in recessive dystrophic EB. Taken together, the processes of subepidermal blister healing highlight HFs as a target for treating the wounds of EB and other blistering diseases.

Our study has some limitations, primarily due to the discrepancies between mice and humans. First, eccrine sweat glands have been reported to contribute to wound healing in human skin (Rittie *et al*, 2013). As murine back skin does not harbor sweat glands, our study was unable to estimate the contribution of the sweat glands in human settings. Second, although the skin-split level of human recessive dystrophic EB is generally just beneath lamina densa (basement membrane), as was the case for the *Col7a1*$^{-/-}$ blisters in our study, suction blistering on human recessive dystrophic EB induces skin detachment in the lamina lucida, that is, between hemidesmosomes and the lamina densa (Tidman & Eady, 1984). In addition, our study did not look into the contribution of mesenchymal cells to blister healing, which has been described in previous studies on epidermolysis bullosa (Chino *et al*, 2008; Fujita *et al*, 2010; Iinuma *et al*, 2015; Tamai *et al*, 2011; Tolar *et al*, 2009; Webber *et al*, 2017). Further studies are warranted to elucidate the role of mesenchymal cells in blister healing.

In closing, our study has revealed the imbalance between development and wound regeneration in the skin blisters. Our findings of the healing processes pave the way for tailored therapeutic interventions for epidermolysis bullosa, pemphigoid diseases and other blistering diseases.

Material and Methods

Animals

C57BL/6 strain mice were purchased from Clea (Tokyo, Japan). Ins-Topgal+ mice were obtained from RIKEN BRC (Tsukuba, Japan) (Moriyama *et al*, 2007). K14CreER, Lrig1CreER, and R26R-confetti mice were purchased from the Jackson Laboratory (Bar Harbor, Maine, USA). R26R-H2B-mCherry mice were provided by RIKEN (Kobe, Japan). *Col17a1*$^{-/-}$ and hCOL17+;*Col17a1*$^{-/-}$ mice were generated as previously described (Nishie *et al.*, 2007). *Col7a1*$^{-/-}$ mice were provided by Prof. Jouni Uitto (Heinonen *et al.*, 1999). The institutional review board of the Hokkaido University Graduate School of Medicine approved all animal studies described below.

Suction blisters

Suction blisters were produced on the neonatal murine dorsal skin (P1) using a syringe and connector tubes. The negative pressure applied to the skin (generally for minutes) was 523.4±1.3 mmHg (evaluated by an Ex Pocket Pressure Indicator PM-281 (AS ONE, Osaka, Japan)). The diameter of the syringe attached to the skin was 4 mm. The size of the typical blister was 3 mm in diameter.

Histology

Mouse dorsal skin specimens were fixed in formalin and embedded in paraffin after dehydration or were frozen on dry ice in an optimal cutting temperature (OCT) compound. Frozen sections were fixed with 4% paraformaldehyde (PFA) or cold

acetone or were stained without fixation. Antigen retrieval with pH 6.0 (citrate) or pH 9.0 (EDTA) buffer was performed on deparaffinized sections. Sections were incubated with primary antibodies overnight at 4°C. After being washed in phosphate-buffered saline (PBS), the sections were incubated with secondary antibodies conjugated to FITC, Alexa 488, Alexa 647 or Alexa 680 for 1 hr at room temperature (RT). The nuclei were stained with propidium iodide (PI) or 4',6-diamidino-2-phenylindole (DAPI). The stained immunofluorescent samples were observed using a confocal laser scanning microscope (FV-1000 (Olympus, Tokyo, Japan) or LSM-710 (Zeiss, Oberkochen, Germany)).

For immunohistochemistry, horseradish peroxidase (HRP)-tagged secondary antibodies were used. Sections were blocked with hydrogen peroxide, labeled with antibodies, and counterstained with hematoxylin. For morphological analysis, deparaffinized sections were stained with hematoxylin and eosin (H&E) by conventional methods. Alkaline phosphatase staining was performed using a StemAb Alkaline Phosphatase Staining Kit II (Stemgent, San Diego, California, USA). Images of immunohistochemistry, and H&E- and alkaline phosphatase-stained sections were captured with a BZ-9000 microscope (Keyence, Tokyo, Japan).

For whole-mount staining, mouse dorsal skin samples were fixed with 4% PFA and immunolabeled or stained with the Alkaline Phosphatase Staining Kit II. For X-gal staining of ins-Topgal+ mouse skin, a beta-galactosidase staining kit (Takara-bio, Shiga, Japan) was used according to the provider’s protocol. Briefly, dorsal skin samples were fixed with 4% PFA for 1 hr at 4°C and soaked in staining solution overnight at RT. Tissues were mounted in a Mowiol solution. Images were observed with LSM-710, FV-1000 or BZ-9000 microscopes.

HF morphological stages were evaluated as previously described (Paus *et al.*, 1999). The length of the major axis of keratinocytes in the intact and regenerated epidermis was measured using ImageJ (NIH, Bethesda, Maryland, USA) on K14-stained sections. The quantification of the cells expressing a particular marker was performed as previously described (Natsuga *et al*, 2016).

Antibodies

The following antibodies were used: anti-BrdU (Abcam, Cambridge, UK; BU1/75, Dako; M0744), anti-phospho-Histone H3 (Ser10) (Merck Millipore, Billerica, Massachusetts, USA), anti-loricrin (Covance, Princeton, New Jersey, USA), FITC-conjugated anti-CD3e (BioLegend, San Diego, California, USA; 145-2C11), Alexa Fluor 488-conjugated anti-F4/80 (Affymetrix, Santa Clara, California, USA; BM8), FITC (fluorescein isothiocyanate)-conjugated anti-Ly-6G (Beckman Coulter, Brea, California, USA; RB6-8C5), anti-COL4 (Novus Biologicals, Centennial, Colorado; NB120-6586), anti-COL7 (homemade (Iwata *et al*, 2013)), anti- COL17 (Abcam; ab186415), anti-ITGA5 (Abcam; EPR7854), anti-ITGA6 (BD Biosciences Pharmingen, San Diego, California, USA; GoH3), anti-L332 (Abcam; ab14509), anti-laminin β1 (Abcam; ab44941), anti-pan-cytokeratin (PROGEN, Wieblingen, Heidelberg, Germany; PRGN-10550), anti-cytokeratin 10 (Biolegend; Poly19054), anti-cytokeratin 14 (ThermoFisher, Waltham, Massachusetts, USA; LL002).

BrdU labeling

For proliferation analysis, 10 μg of BrdU (BD Biosciences Pharmingen) per head was intraperitoneally administered 4 hr before sacrifice.

Transmission electron microscopy

The samples were taken from C57BL/6 mouse dorsal skin (P1) just after suction blistering was performed. The samples were fixed in 5% glutaraldehyde solution, postfixed in 1% OsO_4, dehydrated, and embedded in Epon 812. The embedded samples were sectioned at 1 μm thickness for light microscopy and thin-sectioned for electron microscopy (70 nm thick). The thin sections were stained with uranyl acetate and lead citrate and examined by transmission electron microscopy (H-7100; Hitachi, Tokyo, Japan).

Lineage tracing

K14CreER:R26R-H2B-mCherry, Lrig1CreER:R26R-H2B-mCherry, K14CreER:R26R-confetti, and Lrig1CreER:R26R-confetti mice were intraperitoneally treated with 0.5 mg of tamoxifen (T5648; Sigma-Aldrich, St. Louis, Missouri, USA) at P0. The dorsal skin samples were harvested four days later (P4).

RNA sequencing and analysis

Suction-blistered and control samples were collected at P2 at the same time of day to exclude the effects of circadian oscillations on epidermal gene expression (Janich *et al*, 2013). The skin samples were treated with 0.25% trypsin EDTA overnight at 4°C. The blistered and regenerated epidermis was collected by separating it from the dermis,

minced with a scalpel and suspended in 10% FCS DMEM. The cell suspension was filtered through a 70 μm filter, and cell pellets were collected. Library preparation was performed using an Illumina TruSeq RNA prep kit by following the manufacturer's instructions. Briefly, following TRIzol extraction and chemical fragmentation, mRNA was purified with oligo-dT-attached magnetic beads and reverse transcribed into cDNA. Following a second strand synthesis step with DNA polymerase I and RNAse H, the resulting cDNA was subjected to end repair, A-tailing, and Illumina compatible adaptor ligation. Following purification and PCR-mediated enrichment, libraries were purified with AMPure XP beads and sequenced on a NextSeq 500 Illumina sequencer.

After quality controls were performed, the raw reads were aligned to the NCBIm37 mouse reference genome (mm9) using HiSat2 (Kim *et al*, 2015) (version 2.0.0) using options -N 1 -L 20 -i S, 1, 0.5 -D 25 -R 5 --pen-noncansplice 20 --mp 1, 0 --sp 3, 0 and providing a list of known splice sites. Expression levels were quantified using featureCounts (Liao *et al*, 2014) with RefSeq gene annotation and normalized as TPM using custom scripts. Differential expression analysis was performed using the edgeR (Robinson *et al*, 2010) software package. After lowly expressed genes (1 count per million in less than two samples) were filtered out, the treatment and control groups were compared using the exact test method (Robinson *et al.*, 2010). Genes with an absolute log2-fold change greater than 1 and false discovery rate (FDR) less than or equal to 0.05 were considered differentially expressed. Hierarchical clustering of gene expression profiles was performed on differentially expressed genes using only Euclidean distances and the complete linkage method. TPM values were normalized as Z-scores across samples, and the distances were computed. GO term, KEGG pathway

enrichment analysis on differentially expressed genes and GO term network visualization were performed using the clusterProfiler R/Bioconductor package (Yu *et al*, 2012). To validate the enriched pathways, GSEA analysis was performed.

Intrablister administration

Ten microliters of 1.8 or 9.0 mM $CaCl_2$ in PBS was administered by syringe into the blisters just after the suction blistering procedure was performed.

Statistics

Statistical analyses were performed using GraphPad Prism (GraphPad Software, La Jolla, California, USA). P-values were determined using Student's t-test or one-way ANOVA followed by Tukey's test. P-values are indicated as *0.01<p<0.05, **0.001<p<0.01, ***0.0001<p<0.001, and ****p<0.0001. The values were shown as the means ± standard errors (SE), violin plots or connected with lines showing individual mice.

Mathematical modeling

A mathematical model proposed for epidermal cell dynamics (Kobayashi *et al.*, 2016; Kobayashi *et al.*, 2018) was adapted to simulate epidermal wound healing. (For the detailed mathematical formulation, see the Appendix Supplementary Methods and **Dataset EV2**.) In this model, epidermal basal cells were represented as spherical particles, with the cell diameter set to 10 μm. Cells designated as epidermal SCs and their progeny could undergo division on the basement membrane. Cell division was

described as a process of two initially completely overlapping particles gradually separating into two distinct particles. When a newly created cell was not fully surrounded by other cells, it was judged as being in a regeneration process and immediately underwent a transition to an oblate spheroid shape with the long axis increased by a factor of 2 (normal) or 1.5 (simulating *Col7a1*$^{-/-}$ and Ca-treated blisters) while its volume was kept constant. The same division rate was assigned to all proliferative cells, with an average division period of 57.6 [arb. unit]. Forces exerted on a cell came from adhesion and excluded-volume interactions with other cells and with the basement membrane. SCs were tightly bound and unable to detach from the basement membrane, while the progeny were weakly bound so that they could detach from the membrane via the ambient pressure: the detached cells were removed from the system. The basement membrane was assumed to be a rigid flat surface, whose shape remained unchanged over time. These interactions were calculated to obtain the time evolution of the whole system by solving equations given in a previous report (Kobayashi *et al.*, 2018). The simulation region was set to 600 μm x 600 μm horizontally with periodic boundary conditions. To prepare the initial conditions for the simulation of subepidermal blister healing, we first ran a simulation with SCs placed on the basement membrane until their progeny covered the whole surface. Then, we set the progeny to be nonproliferative and created epidermal defects by removing the cells that were inside a disk domain with a diameter of 480 μm.

Human samples

From the H&E-stained skin of patients with congenital or autoimmune subepidermal blistering diseases (73 EB or 188 bullous pemphigoid (BP) samples, respectively), the samples that met the following histological criteria were selected: (1) subepidermal blisters or a skin split at the dermoepidermal junction; (2) re-epithelization in the area; and (3) presence of HFs on the blister base. Three BP samples fulfilled all the criteria (blisters 1, 2, and 3) and were observed with a Keyence BZ-9000 microscope. The institutional review board of the Hokkaido University Graduate School of Medicine approved all human studies described above (ID: 13-043 and 15-052). The study was conducted according to the Declaration of Helsinki Principles. Participants or their legal guardians provided written informed consent.

Data availability

The datasets produced in this study are available in the following databases:

- RNA-Seq data: Gene Expression Omnibus GSE154871 (https://www.ncbi.nlm.nih.gov/geo/query/acc.cgi?acc=GSE154871)

Author contributions

Y. F. designed and performed the experiments, analyzed the data, interpreted the results, and wrote the manuscript. M. W., S. T., H. N., H. K., Y. W., Y. M, A. L., V. P., H. U., H. I., W. N., and S. O. performed the experiments and analyzed the data. K. O., Y. K., and M. N. performed the mathematical modeling and wrote the manuscript. G. D. designed and performed the experiments, analyzed the data and interpreted the results.

H. S. interpreted the results and supervised the study. K. N. conceived and designed the experiments, analyzed the data, interpreted the results, wrote the manuscript and supervised the study.

Acknowledgments

We thank Ms. Meari Yoshida and Ms. Megumi Takehara for their technical assistance. We also thank Professor Yumiko Saga, Professor Kim B Yancey, and Professor Jouni Uitto for providing the ins-Topgal+, K14-hCOL17, and *Col7a1*$^{-/-}$ mice, respectively. This work was funded by AMED (ID: 18059057), JSPS (KAKEN 17K16317), the Uehara Foundation, the Lydia O'Leary Memorial Pias Dermatological Foundation to KN, JST CREST (JPMJCR15D2) to MN, JSPS (KAKEN 16K10120) to HN, AIRC IG 20240 to SO, and AIRC MFAG 2018 (ID: 21640) to GD. HS, the senior author of this paper, sadly died while this manuscript was in revision. We dedicate this paper to him.

Conflict of interest

The authors declare that they have no conflict of interest.

References

Aragona M, Dekoninck S, Rulands S, Lenglez S, Mascre G, Simons BD, Blanpain C (2017) Defining stem cell dynamics and migration during wound healing in mouse skin epidermis. *Nat Commun* 8: 14684

Brakebusch C, Grose R, Quondamatteo F, Ramirez A, Jorcano JL, Pirro A, Svensson M, Herken R, Sasaki T, Timpl R *et al* (2000) Skin and hair follicle integrity is crucially dependent on beta 1 integrin expression on keratinocytes. *EMBO J* 19: 3990-4003

Chen M, Kasahara N, Keene DR, Chan L, Hoeffler WK, Finlay D, Barcova M, Cannon PM, Mazurek C, Woodley DT (2002) Restoration of type VII collagen expression and function in dystrophic epidermolysis bullosa. *Nat Genet* 32: 670-675

Chen M, O'Toole EA, Muellenhoff M, Medina E, Kasahara N, Woodley DT (2000) Development and characterization of a recombinant truncated type VII collagen "minigene". Implication for gene therapy of dystrophic epidermolysis bullosa. *J Biol Chem* 275: 24429-24435

Chen X, Cai G, Liu C, Zhao J, Gu C, Wu L, Hamilton TA, Zhang CJ, Ko J, Zhu L *et al* (2019) IL-17R-EGFR axis links wound healing to tumorigenesis in Lrig1(+) stem cells. *J Exp Med* 216: 195-214

Chetty BV, Boissy RE, Warden GD, Nordlund JJ (1992) Basement membrane and fibroblast aberration in blisters at the donor, graft, and spontaneously healed sites in patients with burns. *Arch Dermatol* 128: 181-186

Chino T, Tamai K, Yamazaki T, Otsuru S, Kikuchi Y, Nimura K, Endo M, Nagai M, Uitto J, Kitajima Y *et al* (2008) Bone marrow cell transfer into fetal circulation can ameliorate

genetic skin diseases by providing fibroblasts to the skin and inducing immune tolerance. *Am J Pathol* 173: 803-814

Christiano AM, Greenspan DS, Hoffman GG, Zhang X, Tamai Y, Lin AN, Dietz HC, Hovnanian A, Uitto J (1993) A missense mutation in type VII collagen in two affected siblings with recessive dystrophic epidermolysis bullosa. *Nat Genet* 4: 62-66

Dekoninck S, Blanpain C (2019) Stem cell dynamics, migration and plasticity during wound healing. *Nat Cell Biol* 21: 18-24

Donati G, Rognoni E, Hiratsuka T, Liakath-Ali K, Hoste E, Kar G, Kayikci M, Russell R, Kretzschmar K, Mulder KW *et al* (2017) Wounding induces dedifferentiation of epidermal Gata6(+) cells and acquisition of stem cell properties. *Nat Cell Biol* 19: 603-613

Donati G, Watt FM (2015) Stem cell heterogeneity and plasticity in epithelia. *Cell Stem Cell* 16: 465-476

Fernandez Vallone V, Leprovots M, Strollo S, Vasile G, Lefort A, Libert F, Vassart G, Garcia MI (2016) Trop2 marks transient gastric fetal epithelium and adult regenerating cells after epithelial damage. *Development* 143: 1452-1463

Fine JD, Bruckner-Tuderman L, Eady RA, Bauer EA, Bauer JW, Has C, Heagerty A, Hintner H, Hovnanian A, Jonkman MF *et al* (2014) Inherited epidermolysis bullosa: updated recommendations on diagnosis and classification. *J Am Acad Dermatol* 70: 1103-1126

Fujita Y, Abe R, Inokuma D, Sasaki M, Hoshina D, Natsuga K, Nishie W, McMillan JR, Nakamura H, Shimizu T *et al* (2010) Bone marrow transplantation restores epidermal

basement membrane protein expression and rescues epidermolysis bullosa model mice. *Proc Natl Acad Sci U S A* 107: 14345-14350

Garcin CL, Ansell DM, Headon DJ, Paus R, Hardman MJ (2016) Hair Follicle Bulge Stem Cells Appear Dispensable for the Acute Phase of Wound Re-epithelialization. *Stem Cells* 34: 1377-1385

Gay D, Kwon O, Zhang Z, Spata M, Plikus MV, Holler PD, Ito M, Yang Z, Treffeisen E, Kim CD *et al* (2013) Fgf9 from dermal gammadelta T cells induces hair follicle neogenesis after wounding. *Nat Med* 19: 916-923

Gonzales KAU, Fuchs E (2017) Skin and Its Regenerative Powers: An Alliance between Stem Cells and Their Niche. *Dev Cell* 43: 387-401

Heinonen S, Mannikko M, Klement JF, Whitaker-Menezes D, Murphy GF, Uitto J (1999) Targeted inactivation of the type VII collagen gene (Col7a1) in mice results in severe blistering phenotype: a model for recessive dystrophic epidermolysis bullosa. *J Cell Sci* 112 (Pt 21): 3641-3648

Hennings H, Michael D, Cheng C, Steinert P, Holbrook K, Yuspa SH (1980) Calcium regulation of growth and differentiation of mouse epidermal cells in culture. *Cell* 19: 245-254

Hertle MD, Kubler MD, Leigh IM, Watt FM (1992) Aberrant integrin expression during epidermal wound healing and in psoriatic epidermis. *J Clin Invest* 89: 1892-1901

Hilal L, Rochat A, Duquesnoy P, Blanchet-Bardon C, Wechsler J, Martin N, Christiano AM, Barrandon Y, Uitto J, Goossens M *et al* (1993) A homozygous insertion-deletion in the type VII collagen gene (COL7A1) in Hallopeau-Siemens dystrophic epidermolysis bullosa. *Nat Genet* 5: 287-293

679 Iinuma S, Aikawa E, Tamai K, Fujita R, Kikuchi Y, Chino T, Kikuta J, McGrath JA, Uitto
680 J, Ishii M *et al* (2015) Transplanted bone marrow-derived circulating PDGFRalpha+ cells
681 restore type VII collagen in recessive dystrophic epidermolysis bullosa mouse skin graft.
682 *J Immunol* 194: 1996-2003
683 Ito M, Liu Y, Yang Z, Nguyen J, Liang F, Morris RJ, Cotsarelis G (2005) Stem cells in
684 the hair follicle bulge contribute to wound repair but not to homeostasis of the epidermis.
685 *Nat Med* 11: 1351-1354
686 Ito M, Yang Z, Andl T, Cui C, Kim N, Millar SE, Cotsarelis G (2007) Wnt-dependent de
687 novo hair follicle regeneration in adult mouse skin after wounding. *Nature* 447: 316-320
688 Iwata H, Bieber K, Tiburzy B, Chrobok N, Kalies K, Shimizu A, Leineweber S, Ishiko A,
689 Vorobyev A, Zillikens D *et al* (2013) B cells, dendritic cells, and macrophages are
690 required to induce an autoreactive CD4 helper T cell response in experimental
691 epidermolysis bullosa acquisita. *J Immunol* 191: 2978-2988
692 Janich P, Toufighi K, Solanas G, Luis NM, Minkwitz S, Serrano L, Lehner B, Benitah SA
693 (2013) Human epidermal stem cell function is regulated by circadian oscillations. *Cell*
694 *Stem Cell* 13: 745-753
695 Kang S, Long K, Wang S, Sada A, Tumbar T (2020) Histone H3 K4/9/27 Trimethylation
696 Levels Affect Wound Healing and Stem Cell Dynamics in Adult Skin. *Stem Cell Reports*
697 14: 34-48
698 Kiistala U, Mustakallio KK (1964) In-Vivo Separation of Epidermis by Production of
699 Suction Blisters. *Lancet* 2: 1444-1445

Kiistala U, Mustakallio KK (1967) Dermo-epidermal separation with suction. Electron microscopic and histochemical study of initial events of blistering on human skin. *J Invest Dermatol* 48: 466-477

Kim D, Langmead B, Salzberg SL (2015) HISAT: a fast spliced aligner with low memory requirements. *Nat Methods* 12: 357-360

Kobayashi Y, Sawabu Y, Kitahata H, Denda M, Nagayama M (2016) Mathematical model for calcium-assisted epidermal homeostasis. *J Theor Biol* 397: 52-60

Kobayashi Y, Yasugahira Y, Kitahata H, Watanabe M, Natsuga K, Nagayama M (2018) Interplay between epidermal stem cell dynamics and dermal deformation. *npj Computational Materials* 4: 45

Krawczyk WS (1971) A pattern of epidermal cell migration during wound healing. *J Cell Biol* 49: 247-263

Lane EB, Wilson CA, Hughes BR, Leigh IM (1991) Stem cells in hair follicles. Cytoskeletal studies. *Ann N Y Acad Sci* 642: 197-213

Leivo T, Kiistala U, Vesterinen M, Owaribe K, Burgeson RE, Virtanen I, Oikarinen A (2000) Re-epithelialization rate and protein expression in the suction-induced wound model: comparison between intact blisters, open wounds and calcipotriol-pretreated open wounds. *Br J Dermatol* 142: 991-1002

Liao Y, Smyth GK, Shi W (2014) featureCounts: an efficient general purpose program for assigning sequence reads to genomic features. *Bioinformatics* 30: 923-930

Liu N, Matsumura H, Kato T, Ichinose S, Takada A, Namiki T, Asakawa K, Morinaga H, Mohri Y, De Arcangelis A *et al* (2019) Stem cell competition orchestrates skin homeostasis and ageing. *Nature*

723 Magee AI, Lytton NA, Watt FM (1987) Calcium-induced changes in cytoskeleton and
724 motility of cultured human keratinocytes. *Exp Cell Res* 172: 43-53
725 Matsumura H, Mohri Y, Binh NT, Morinaga H, Fukuda M, Ito M, Kurata S, Hoeijmakers
726 J, Nishimura EK (2016) Hair follicle aging is driven by transepidermal elimination of
727 stem cells via COL17A1 proteolysis. *Science* 351: aad4395
728 McGrath JA, Gatalica B, Christiano AM, Li K, Owaribe K, McMillan JR, Eady RA, Uitto J
729 (1995) Mutations in the 180-kD bullous pemphigoid antigen (BPAG2), a
730 hemidesmosomal transmembrane collagen (COL17A1), in generalized atrophic benign
731 epidermolysis bullosa. *Nat Genet* 11: 83-86
732 McMillan JR, Akiyama M, Shimizu H (2003) Epidermal basement membrane zone
733 components: ultrastructural distribution and molecular interactions. *J Dermatol Sci* 31:
734 169-177
735 Miao Q, Hill MC, Chen F, Mo Q, Ku AT, Ramos C, Sock E, Lefebvre V, Nguyen H
736 (2019) SOX11 and SOX4 drive the reactivation of an embryonic gene program during
737 murine wound repair. *Nat Commun* 10: 4042
738 Moriyama A, Kii I, Sunabori T, Kurihara S, Takayama I, Shimazaki M, Tanabe H,
739 Oginuma M, Fukayama M, Matsuzaki Y *et al* (2007) GFP transgenic mice reveal active
740 canonical Wnt signal in neonatal brain and in adult liver and spleen. *Genesis* 45: 90-100
741 Natsuga K (2014) Epidermal barriers. *Cold Spring Harb Perspect Med* 4: a018218
742 Natsuga K, Cipolat S, Watt FM (2016) Increased Bacterial Load and Expression of
743 Antimicrobial Peptides in Skin of Barrier-Deficient Mice with Reduced Cancer
744 Susceptibility. *J Invest Dermatol* 136: 99-106

745 Natsuga K, Watanabe M, Nishie W, Shimizu H (2019) Life before and beyond blistering:
746 The role of collagen XVII in epidermal physiology. *Exp Dermatol* 28: 1135-1141
747 Niculescu C, Ganguli-Indra G, Pfister V, Dupe V, Messaddeq N, De Arcangelis A,
748 Georges-Labouesse E (2011) Conditional ablation of integrin alpha-6 in mouse
749 epidermis leads to skin fragility and inflammation. *Eur J Cell Biol* 90: 270-277
750 Nishie W, Sawamura D, Goto M, Ito K, Shibaki A, McMillan JR, Sakai K, Nakamura H,
751 Olasz E, Yancey KB *et al* (2007) Humanization of autoantigen. *Nat Med* 13: 378-383
752 Nusse YM, Savage AK, Marangoni P, Rosendahl-Huber AKM, Landman TA, de
753 Sauvage FJ, Locksley RM, Klein OD (2018) Parasitic helminths induce fetal-like
754 reversion in the intestinal stem cell niche. *Nature* 559: 109-113
755 Nystrom A, Velati D, Mittapalli VR, Fritsch A, Kern JS, Bruckner-Tuderman L (2013)
756 Collagen VII plays a dual role in wound healing. *J Clin Invest* 123: 3498-3509
757 Osaka N, Takahashi T, Murakami S, Matsuzawa A, Noguchi T, Fujiwara T, Aburatani H,
758 Moriyama K, Takeda K, Ichijo H (2007) ASK1-dependent recruitment and activation of
759 macrophages induce hair growth in skin wounds. *J Cell Biol* 176: 903-909
760 Page ME, Lombard P, Ng F, Gottgens B, Jensen KB (2013) The epidermis comprises
761 autonomous compartments maintained by distinct stem cell populations. *Cell Stem Cell*
762 13: 471-482
763 Paladini RD, Takahashi K, Bravo NS, Coulombe PA (1996) Onset of re-epithelialization
764 after skin injury correlates with a reorganization of keratin filaments in wound edge
765 keratinocytes: defining a potential role for keratin 16. *J Cell Biol* 132: 381-397

766 Park S, Gonzalez DG, Guirao B, Boucher JD, Cockburn K, Marsh ED, Mesa KR, Brown
767 S, Rompolas P, Haberman AM *et al* (2017) Tissue-scale coordination of cellular
768 behaviour promotes epidermal wound repair in live mice. *Nat Cell Biol* 19: 155-163
769 Paus R, Muller-Rover S, Van Der Veen C, Maurer M, Eichmuller S, Ling G, Hofmann U,
770 Foitzik K, Mecklenburg L, Handjiski B (1999) A comprehensive guide for the recognition
771 and classification of distinct stages of hair follicle morphogenesis. *J Invest Dermatol*
772 113: 523-532
773 Rittie L, Sachs DL, Orringer JS, Voorhees JJ, Fisher GJ (2013) Eccrine sweat glands
774 are major contributors to reepithelialization of human wounds. *Am J Pathol* 182: 163-
775 171
776 Robinson MD, McCarthy DJ, Smyth GK (2010) edgeR: a Bioconductor package for
777 differential expression analysis of digital gene expression data. *Bioinformatics* 26: 139-
778 140
779 Rognoni E, Gomez C, Pisco AO, Rawlins EL, Simons BD, Watt FM, Driskell RR (2016)
780 Inhibition of beta-catenin signalling in dermal fibroblasts enhances hair follicle
781 regeneration during wound healing. *Development* 143: 2522-2535
782 Rognoni E, Watt FM (2018) Skin Cell Heterogeneity in Development, Wound Healing,
783 and Cancer. *Trends Cell Biol* 28: 709-722
784 Sada A, Jacob F, Leung E, Wang S, White BS, Shalloway D, Tumbar T (2016) Defining
785 the cellular lineage hierarchy in the interfollicular epidermis of adult skin. *Nat Cell Biol*
786 18: 619-631
787 Saxena N, Mok KW, Rendl M (2019) An updated classification of hair follicle
788 morphogenesis. *Exp Dermatol* 28: 332-344

789 Schmidt E, Zillikens D (2013) Pemphigoid diseases. *Lancet* 381: 320-332

790 Shimizu H, Ishiko A, Masunaga T, Kurihara Y, Sato M, Bruckner-Tuderman L,
791 Nishikawa T (1997) Most anchoring fibrils in human skin originate and terminate in the
792 lamina densa. *Lab Invest* 76: 753-763

793 Tamai K, Yamazaki T, Chino T, Ishii M, Otsuru S, Kikuchi Y, Iinuma S, Saga K, Nimura
794 K, Shimbo T *et al* (2011) PDGFRalpha-positive cells in bone marrow are mobilized by
795 high mobility group box 1 (HMGB1) to regenerate injured epithelia. *Proc Natl Acad Sci*
796 *U S A* 108: 6609-6614

797 Tang DD, Gerlach BD (2017) The roles and regulation of the actin cytoskeleton,
798 intermediate filaments and microtubules in smooth muscle cell migration. *Respir Res*
799 18: 54

800 Tanimura S, Tadokoro Y, Inomata K, Binh NT, Nishie W, Yamazaki S, Nakauchi H,
801 Tanaka Y, McMillan JR, Sawamura D *et al* (2011) Hair follicle stem cells provide a
802 functional niche for melanocyte stem cells. *Cell Stem Cell* 8: 177-187

803 Tidman MJ, Eady RA (1984) Evidence for a functional defect of the lamina lucida in
804 recessive dystrophic epidermolysis bullosa demonstrated by suction blisters. *Br J*
805 *Dermatol* 111: 379-387

806 Tolar J, Ishida-Yamamoto A, Riddle M, McElmurry RT, Osborn M, Xia L, Lund T,
807 Slattery C, Uitto J, Christiano AM *et al* (2009) Amelioration of epidermolysis bullosa by
808 transfer of wild-type bone marrow cells. *Blood* 113: 1167-1174

809 Tosti A, Duque-Estrada B, Murrell DF (2010) Alopecia in epidermolysis bullosa.
810 *Dermatol Clin* 28: 165-169

Uroz M, Garcia-Puig A, Tekeli I, Elosegui-Artola A, Abenza JF, Marin-Llaurado A, Pujals S, Conte V, Albertazzi L, Roca-Cusachs P *et al* (2019) Traction forces at the cytokinetic ring regulate cell division and polyploidy in the migrating zebrafish epicardium. *Nat Mater* 18: 1015-1023

Vahidnezhad H, Youssefian L, Saeidian AH, Uitto J (2019) Phenotypic Spectrum of Epidermolysis Bullosa: The Paradigm of Syndromic versus Non-Syndromic Skin Fragility Disorders. *J Invest Dermatol* 139: 522-527

Watanabe M, Natsuga K, Nishie W, Kobayashi Y, Donati G, Suzuki S, Fujimura Y, Tsukiyama T, Ujiie H, Shinkuma S *et al* (2017) Type XVII collagen coordinates proliferation in the interfollicular epidermis. *Elife* 6

Watanabe M, Natsuga K, Shinkuma S, Shimizu H (2018) Epidermal aspects of type VII collagen: Implications for dystrophic epidermolysis bullosa and epidermolysis bullosa acquisita. *J Dermatol* 45: 515-521

Watt FM, Fujiwara H (2011) Cell-extracellular matrix interactions in normal and diseased skin. *Cold Spring Harb Perspect Biol* 3

Webber BR, O'Connor KT, McElmurry RT, Durgin EN, Eide CR, Lees CJ, Riddle MJ, Mathews WE, Frank NY, Kluth MA *et al* (2017) Rapid generation of Col7a1(-/-) mouse model of recessive dystrophic epidermolysis bullosa and partial rescue via immunosuppressive dermal mesenchymal stem cells. *Lab Invest* 97: 1218-1224

White KD, Abe R, Ardern-Jones M, Beachkofsky T, Bouchard C, Carleton B, Chodosh J, Cibotti R, Davis R, Denny JC *et al* (2018) SJS/TEN 2017: Building Multidisciplinary Networks to Drive Science and Translation. *J Allergy Clin Immunol Pract* 6: 38-69

Yu G, Wang LG, Han Y, He QY (2012) clusterProfiler: an R package for comparing biological themes among gene clusters. *OMICS* 16: 284-287

Yui S, Azzolin L, Maimets M, Pedersen MT, Fordham RP, Hansen SL, Larsen HL, Guiu J, Alves MRP, Rundsten CF *et al* (2018) YAP/TAZ-Dependent Reprogramming of Colonic Epithelium Links ECM Remodeling to Tissue Regeneration. *Cell Stem Cell* 22: 35-49 e37

Figure Legends

Figure 1. Healing of subepidermal blisters in neonatal mice.

A Schematic diagram of suction blistering and sample collection. A blister produced on C57BL/6 wild-type (WT) mouse dorsal skin at P1. BM: basement membrane.

B-D Blistered samples at P1. (B) Hematoxylin and eosin (H&E, top) and alkaline phosphatase (AP, bottom) staining. Hair follicles (HFs) remaining in the dermis (indicated by arrows). Scale bar: 500 μm. (C) α6 Integrin (ITGA6, indicated by arrowheads) and type IV collagen (COL4, arrows) labeling (left). Laminin 332 (L332, arrows) staining (right). Scale bar: 100 μm. (D) Ultrastructural findings of blistered skin (left image: blister roof, right image: blister bottom) . Hemidesmosomes (white arrowheads) and lamina densa (arrows) are indicated. Scale bar: 1 μm.

E H&E (left), pan-cytokeratin (PCK, middle), and ITGA6 staining (right) at P2. The regenerated epidermis is indicated by arrowheads. Scale bar: 200 μm.

F Keratin 14 (K14) and keratin 10 (K10) staining of the nonlesional (intact) and lesional (blistered) skin at P2 (upper images and inlets: sections, lower images: whole-mount imaging). HFs are indicated by arrows in the whole-mount images. Scale bar: 30 μm.

G H&E (top) and loricrin (LOR, bottom) staining at P3. Scale bar: 200 μm.

H H&E (left), PCK (middle), and LOR staining (right) at P4. Scale bar: 200 μm.

Data information: Blisters are indicated by stars. Representative images are shown from three or more replicates in each group.

Figure 2. Delayed HF growth during subepidermal blister healing.

A Heat map (Pearson's correlation) of differentially expressed genes between the blistered (regenerated) and control WT dorsal skin epidermis at P2 (n=3).

B GO analysis of differentially expressed genes in the regenerated epidermis.

C Scatter plots of differentially expressed genes in the regenerated epidermis. The red dots represent upregulated genes, and the blue dots represent downregulated genes. The gray dotted lines indicate |logFC|>1.

D Hair canals in the regenerated (lesional) and nonlesional epidermis at P4 (indicated by asterisks). Scale bar: 300 μm.

E Quantification of hair canals in the lesional, nonlesional, and unaffected littermate control epidermis at P4 (n=5 biological replicates). The data are shown as the mean ± SE (littermate control) or connected with lines showing individual mice. *0.01<p<0.05, one-way ANOVA test, followed by Tukey's test.

F HF morphogenesis stages at P4 in lesional, nonlesional, and unaffected littermate control skin (n=5 biological replicates).

G Whole-mount imaging of the blistered skin of ins-Topgal+ mice at P2. Scale bar: 500 μm.

Data information: Representative images are shown from three or more replicates in each group.

Figure 3. Predominant contribution of HF-derived keratinocytes to subepidermal blister healing.

A (Top) BrdU labeling of blistered samples at P2. Scale bar: 100 μm. BrdU-positive cells are indicated by arrows. Blisters are indicated by stars. (Bottom) Quantification of BrdU-positive cells in the epidermis (left) and HFs (right) (n=4 biological replicates). The data are shown as the mean ± SE. *0.01<p<0.05, one-way ANOVA test, followed by Tukey's test. NS, no significance.

B α5 integrin (ITGA5) labeling at P2 (left image: section, right image: whole-mount). Scale bar: 100 μm. Blister edges (epidermal tongue) and HFs are indicated by arrowheads and arrows, respectively. Blisters are indicated by stars.

C Lineage tracing strategy.

D (Top) Sections of K14CreER:H2B-mCherry mice at P4. Scale bar: 100 μm. (Bottom) Quantification of mCherry-positive cells (n=3).. The data from individual mice are connected by lines. Student's t-test. NS, no significance.

E Whole-mount imaging of K14CreER:R26R-confetti samples at P4. Scale bar: 200 μm.

F (Top) Sections of Lrig1CreER:H2B-mCherry mouse skin at P4. Scale bar: 100 μm. (Bottom) Quantification of mCherry-positive cells (n=3). The data from individual mice are connected by lines. *0.01<p<0.05, Student's t-test.

G Whole-mount imaging of Lrig1CreER:R26R-confetti mouse samples at P4. Scale bar: 200 μm.

Data information: Representative images are shown from three or more replicates in each group.

Figure 4. Effects of HF reduction on subepidermal blister healing.

A Type XVII collagen (COL17, arrowheads indicate the hair bulge) and laminin β1 (LAMB1) labeling in WT dorsal skin sections (P1). Scale bar: 100 μm.

B, C Blistered samples of *Col17a1*$^{-/-}$ mouse dorsal skin at P1. ITGA6 (indicated by arrowheads) and COL4 (arrows) labeling (B). L332 staining (C, arrows). Scale bar: 100 μm.

D H&E staining of blistered skin from *Col17a1*$^{-/-}$ mice at P1. HFs detached from the dermis in *Col17a1*$^{-/-}$ skin are indicated by arrowheads. Scale bar: 500 μm.

E Whole-mount AP staining of the blister roof epidermis from *Col17a1*$^{-/-}$ mice (right) and littermate controls (left) at P1. Scale bar: 500 μm.

F H&E (P2, left), ITGA6 (P2, middle) and LOR staining (P4, right) of *Col17a1*$^{-/-}$ mice (top) and littermate controls (bottom) . The regenerated epidermis is indicated by arrowheads. Scale bar: 200 μm.

G (Top) BrdU labeling of *Col17a1*$^{-/-}$ skin at P2. Scale bar: 100 μm. (Bottom) Quantification of BrdU-positive cells in the epidermis surrounding blisters (n= 3 (control) and 4 (*Col17a1*-/-) biological replicates). The data are shown as the mean ± SE. Student's t-test. NS, no significance.

H, I (H) Lineage tracing of K14CreER:R26R-mCherry:*Col17a1*$^{-/-}$ at P4. Scale bar: 100 μm. (I) Quantification of mCherry-positive cells in the regenerated epidermis (n=3 biological replicates). The data from individual mice are connected by lines. *0.01<p<0.05, Student's t-test.

Data information: Blisters are indicated by stars. Representative images are shown from three or more replicates in each group.

Figure 5. Involvement of keratinocyte shape transformation in subepidermal blister healing.

A Type VII collagen (COL7) labeling in WT dorsal skin sections (P1). Scale bar: 200 μm.

B ITGA6/COL4 (left, indicated by arrows) and L332 labeling (right, indicated by arrows) in the blistered skin of *Col7a1*$^{-/-}$ mice at P1. Scale bar: 100 μm.

C Schematic diagram of control, *Col17a1*$^{-/-}$, and *Col7a1*$^{-/-}$ mouse skin splits. BM: basement membrane.

D H&E staining of blistered skin from *Col7a1*$^{-/-}$ mice (right) and their littermate controls (left) at P1. Scale bar: 200 μm.

E Whole-mount AP staining of the blister roof epidermis from *Col7a1*$^{-/-}$ mice (right) and their littermate controls (left) at P1. Scale bar: 500 μm.

F K10/K14 (low magnification, left) and K14 (high magnification, middle and right) labeling of *Col7a1*$^{-/-}$ mouse (bottom) and littermate control (top) blistered skin at P2. Scale bar: 30 μm.

G Quantification of BrdU-positive cells per μm HF length (n=55 HFs from three control and 143 HFs from four *Col7a1*$^{-/-}$ mice). The data are shown as violin plots. Student's t-test. NS, no significance.

H Length of the major axis of keratinocytes in the regenerated epidermis (n=244 (control, L), and 132 (*Col7a1*$^{-/-}$, L) cells from four mice, respectively) and in the surrounding intact epidermis (basal cells; n=200 (control, NL), 299 (*Col7a1*$^{-/-}$, NL), from four mice, respectively). NL: nonlesional area. L: lesional area. The data are shown as violin plots. ****p<0.0001, one-way ANOVA test, followed by Tukey's test. NS, no significance.

I K10/K14 (left) and K14 (high magnification, right) labeling of WT blistered skin treated with $CaCl_2$ (middle and bottom) or PBS (top) at P2. Scale bar: 30 μm.

J Quantification of BrdU-positive cells per μm HF length (n=83 (PBS), 95 (1.8 mM $CaCl_2$), and 97 (9.0 mM $CaCl_2$) HFs from four mice). One-way ANOVA test, followed by Tukey's test. NS, no significance.

K Length of the major axis of keratinocytes in the regenerated epidermis (n=433 (PBS, L), 451 (1.8 mM $CaCl_2$, L), and 425 (9.0 mM $CaCl_2$, L) cells from four mice) and in the surrounding intact epidermis (basal cells; n=311 (PBS, NL), 279 (1.8 mM $CaCl_2$, NL), 302 (9.0 mM $CaCl_2$, NL) cells from four mice). NL: nonlesional area. L: lesional area. The data are shown as violin plots. ****p<0.0001, one-way ANOVA test, followed by Tukey's test. NS, no significance.

Data information: Blisters are indicated by stars. Representative images are shown from three or more replicates in each group. The dashed and dotted lines in the violin plots show the median and quartiles, respectively.

Figure 6. Mathematical modeling of subepidermal blister healing.

A A particle-based model of subepidermal blister healing at the basal layer. Epidermal basal cells (colored in blue), which do not divide, are placed on the basement membrane (gray). Stem cells (SCs, green) give rise to progeny (simulating HF-derived cells; red) within epidermal defects or in the surrounding epidermis (IFE-derived cells; yellow). t: arbitrary time. See **Movie EV1**.

B Contribution of each progeny cell within the epidermal defect or of surrounding epidermis to subepidermal blister healing, measured as the ratio of the area occupied by each progeny to the area of the initial epidermal defect.

C A model of subepidermal blister healing without SCs within epidermal defects. See **Movie EV2**.

D Time course of subepidermal blister healing in control (A) and SC-depleted epidermal defects (C).

E Effects of the impaired flattening of keratinocytes upon epidermal regeneration. The diameter of basal keratinocytes (long axis of the spheroid) in the regenerated vs. surrounding epidermis was calculated as 1.5:1 (in contrast to 2:1 in Figure 6A). See **Movie EV3**.

F Time course of wound healing for control (A) and less flattened keratinocytes in the regenerated epidermis (E).

Expanded View Figure Legends

Figure EV1. Healing processes of subepidermal blisters.

A H&E (left) and PCK labeling (right) of blistered skin at P1 (WT). Scale bar: 100 μm.

B ITGA6 (arrowheads in the blister roof) and COL4 (arrows in the blister bottom) labeling at P1 (WT). HFs that express ITGA6 on the dermal side are indicated by hashtags. Scale bar: 100 μm (left) and 50 μm (right).

C Electron microscopy of blistered skin at P1 (WT). Hemidesmosomes (white arrowheads) and the lamina densa (arrows) are indicated. Scale bar: 10 μm (left) and 1 μm (right).

D AP staining of WT (left) and *Col17a1*$^{-/-}$ (right) blistered skin at P1. Scale bar: 100 μm.

E H&E (left), ITGA6 (middle), and ITGA5 (right) staining at P2 (WT). The regenerated epidermis is indicated by arrowheads. ITGA5+ cells at the tip of the HFs are indicated by arrows. Blisters are indicated by stars. Scale bar: 100 μm.

F Schematic of the suction blister experiments and HF development/cycles.

G Quantification of immune cells (CD3, F4-80, and Ly6G) in the dermis of blistered WT and unaffected littermate control skin at P2 (n=4 biological replicates) and P4 (n=3 biological replicates). The data are shown as the mean ± SE. *0.01<p<0.05, Student's t-test. NS, no significance.

Data information: Blisters are indicated by stars. Representative images are shown from three or more replicates in each group.

Figure EV2. RNA-seq data on subepidermal blister healing.

A Volcano plot showing differentially expressed genes (DEG) between the blistered (regenerated) and control skin epidermis at P2. Significantly (|LogFC|>1; FDR<0.05) up-regulated and down-regulated DEG are shown in red and blue, respectively.

B Bar plot summarizing GSEA enrichment results for selected up-regulated and down-regulated KEGG pathways. The normalized enrichment score (NES), p-value and FDR are shown.

C GSEA enrichment plots of “Wnt signaling pathway”, “Hedgehog signaling pathway” and “Melanogenesis” KEGG gene sets.

D Network visualization of the top ten down-regulated and up-regulated (FDR<0.05) GO term clusters for different GO categories (Biological process, Molecular Function and Cellular Component). Node size reports the number of enriched genes in each GO term (gene numbers in bottom panels). Nodes are colored as a pie chart depicting the proportion of down-regulated (blue) and up-regulated (red) genes in each GO term. Edge thickness depicts the number of shared genes between GO terms.

Figure EV3. Lineage tracing of subepidermal blister healing.

A Blistered area of K14CreER:R26R-confetti (left) and Lrig1CreER:R26R-confetti (right) mouse skin samples at P4. Scale bar: 100 μm.

B Phospho-Histone H3 (PH3) staining of blistered skin at P2 (WT). Scale bar: 100 μm.

C PH3 staining (arrowhead) of blistered skin at P2 (Lrig1CreER:R26R-H2BmCherry). Scale bar: 100 μm.

D Quantification of mCherry-positive cells during lineage tracing (n=3 biological replicates). The data are shown as the mean ± SE.

Data information: Blisters are indicated by stars. Representative images are shown from three or more replicates in each group.

Figure EV4. Dependence of subepidermal blister healing on flattening ratio and SC arrangement.

A Arrangements of the SCs within epidermal defects (dispersed, 2 cells grouped, 4 cells grouped, and 8 cells grouped) at t = 0.

B Time course of subepidermal blister healing for different keratinocyte flattening ratios (1.0-2.0), each with four SC arrangements.

C Time to full recovery (100% healing rate) for different keratinocyte flattening ratios, averaged over four SC arrangements. The data are shown as the mean ± SD.

Figure EV5. Subepidermal blister healing in humans.

H&E staining of human subepidermal blister samples with re-epithelized areas (blisters 1, 2, and 3). Blisters are indicated by stars. The regenerated epidermis from HFs is indicated by arrows. Scale bar: 300 μm.

Figure 1. Healing of subepidermal blisters in neonatal mice

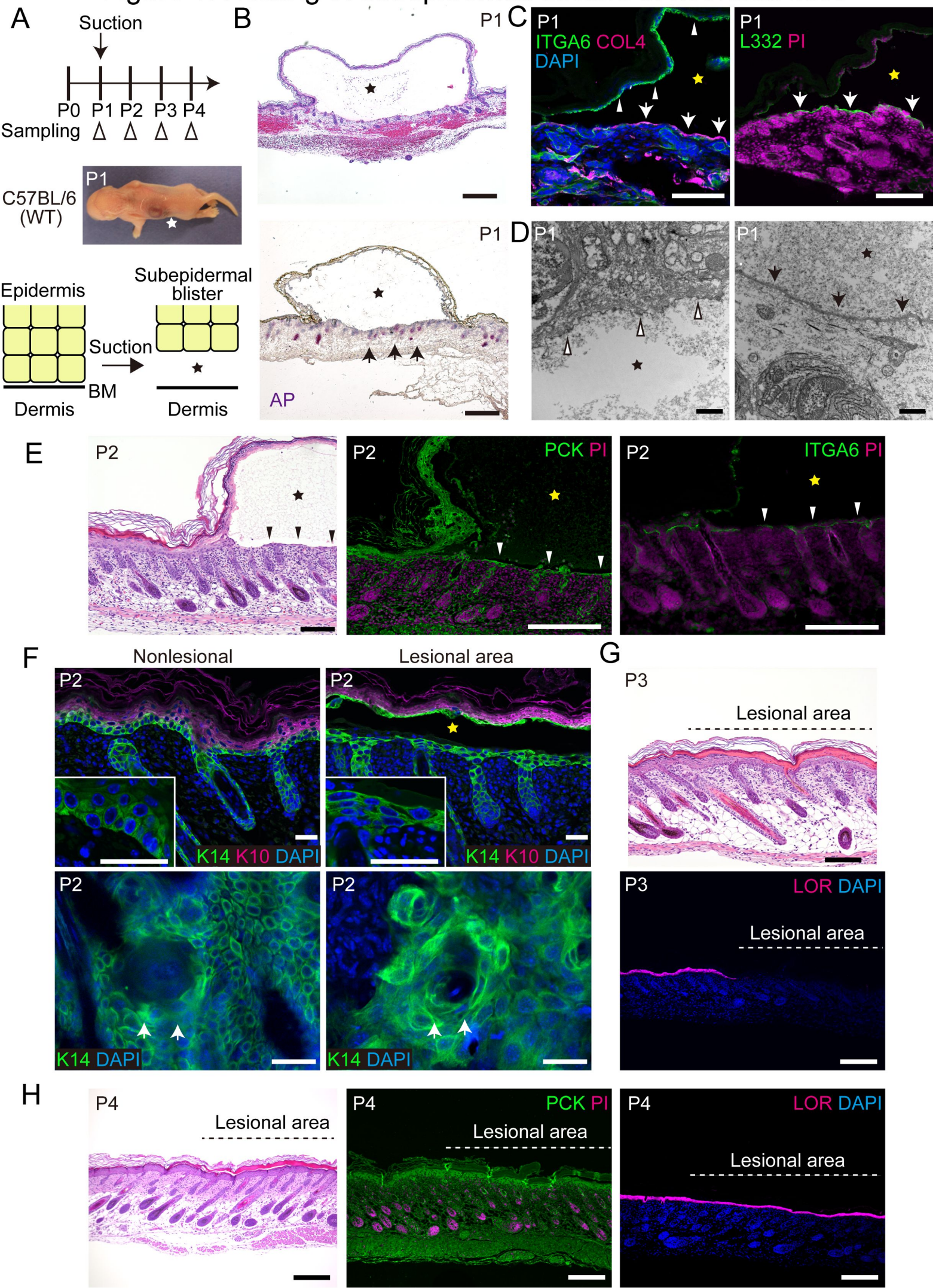

Figure 2. Delayed HF development during subepidermal blister healing

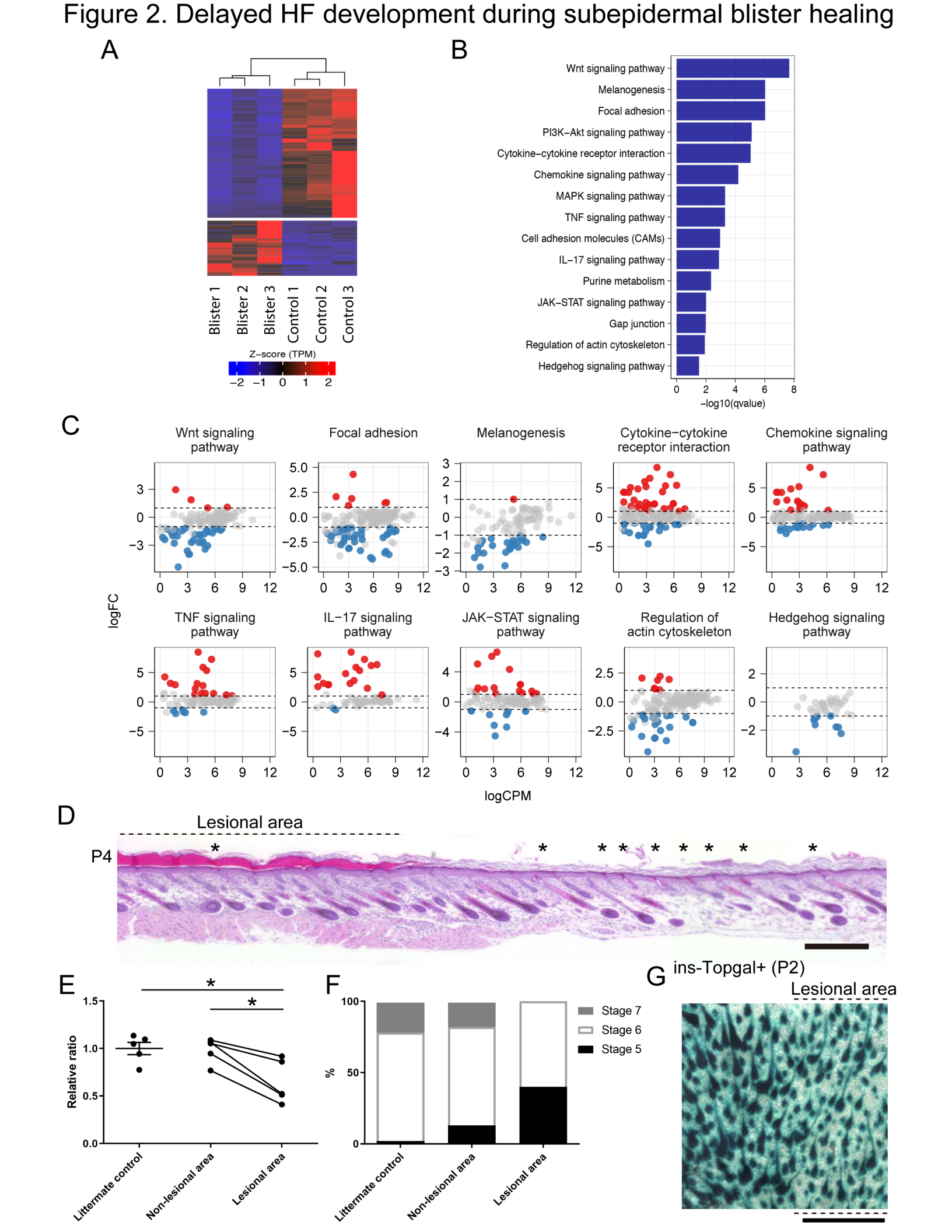

Figure 3. Predominant contribution of HF-derived keratinocytes to subepidermal blister healing

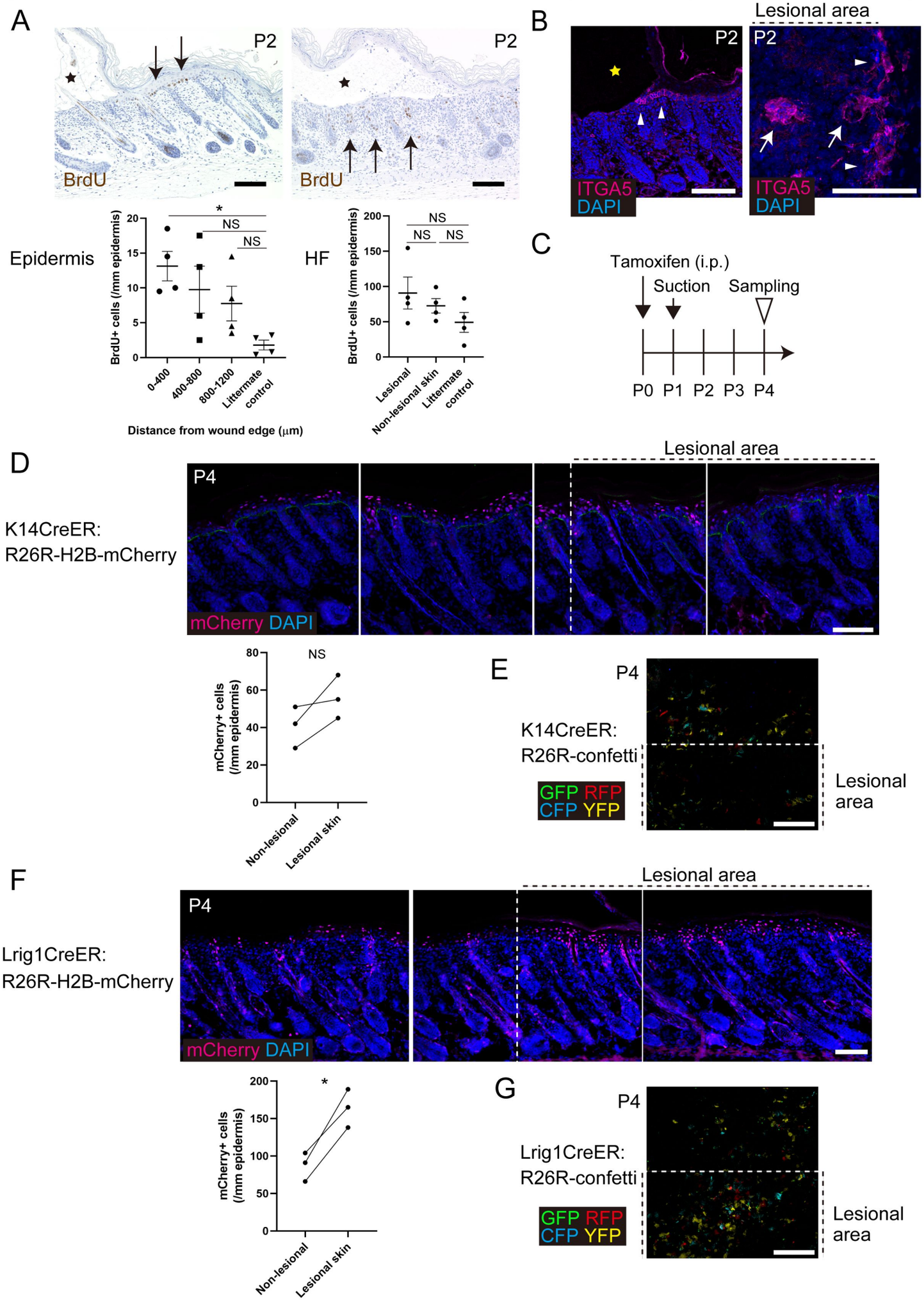

Figure 4. Effects of HF reduction on subepidermal blister healing

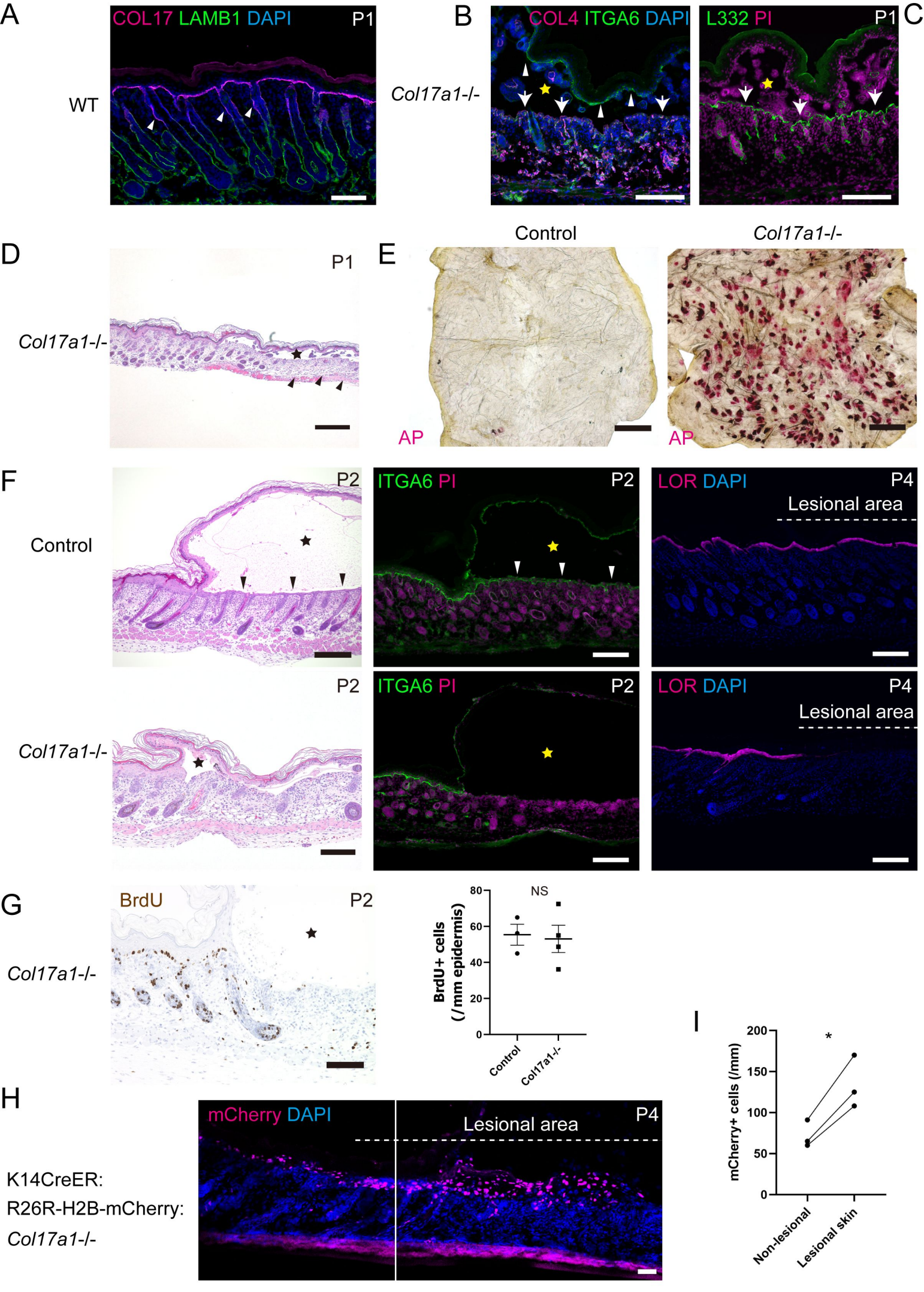

Figure 5. Involvement of keratinocyte shape transformation in subepidermal blister healing

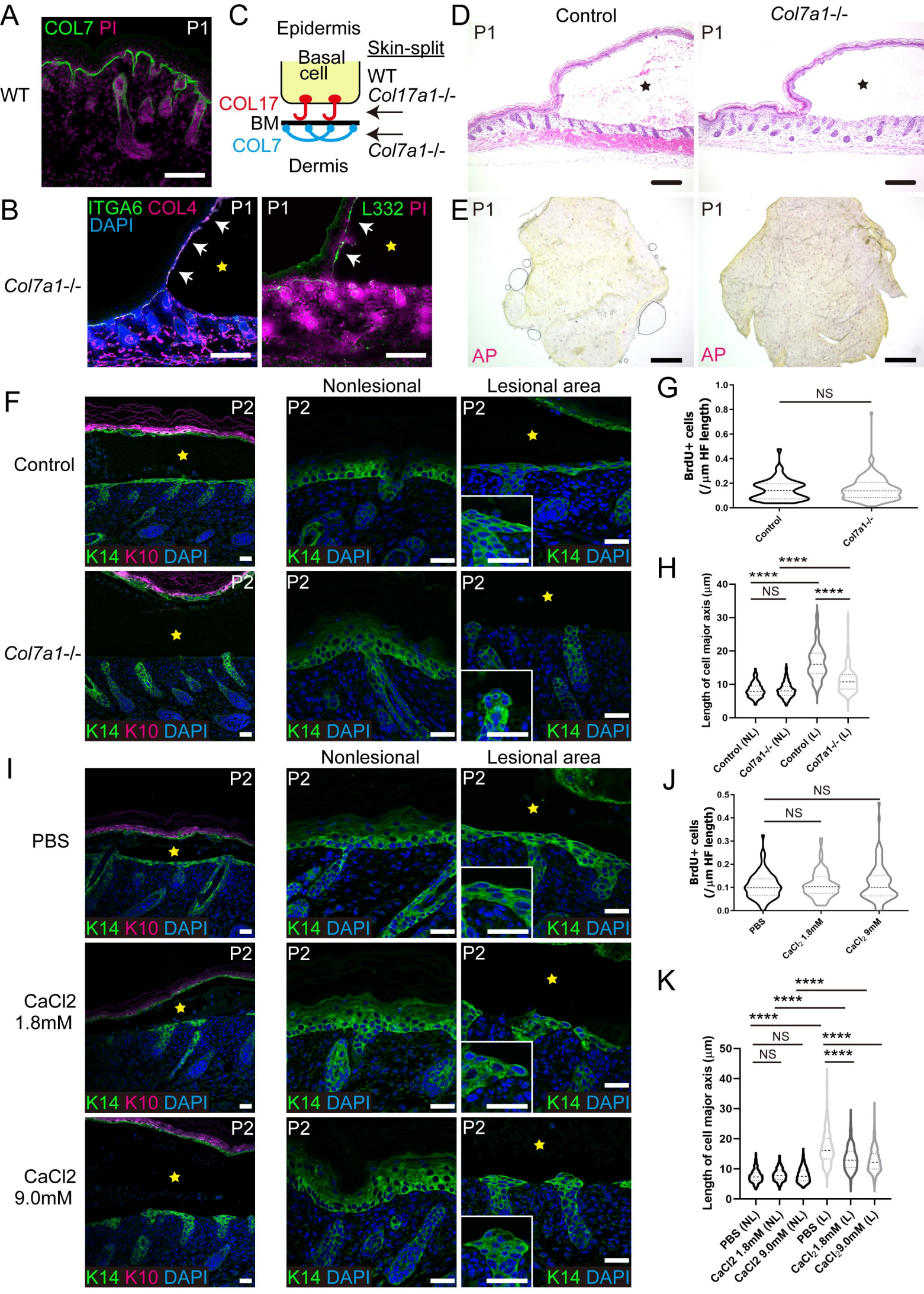

Figure 6. Mathematical modeling of subepidermal blister healing

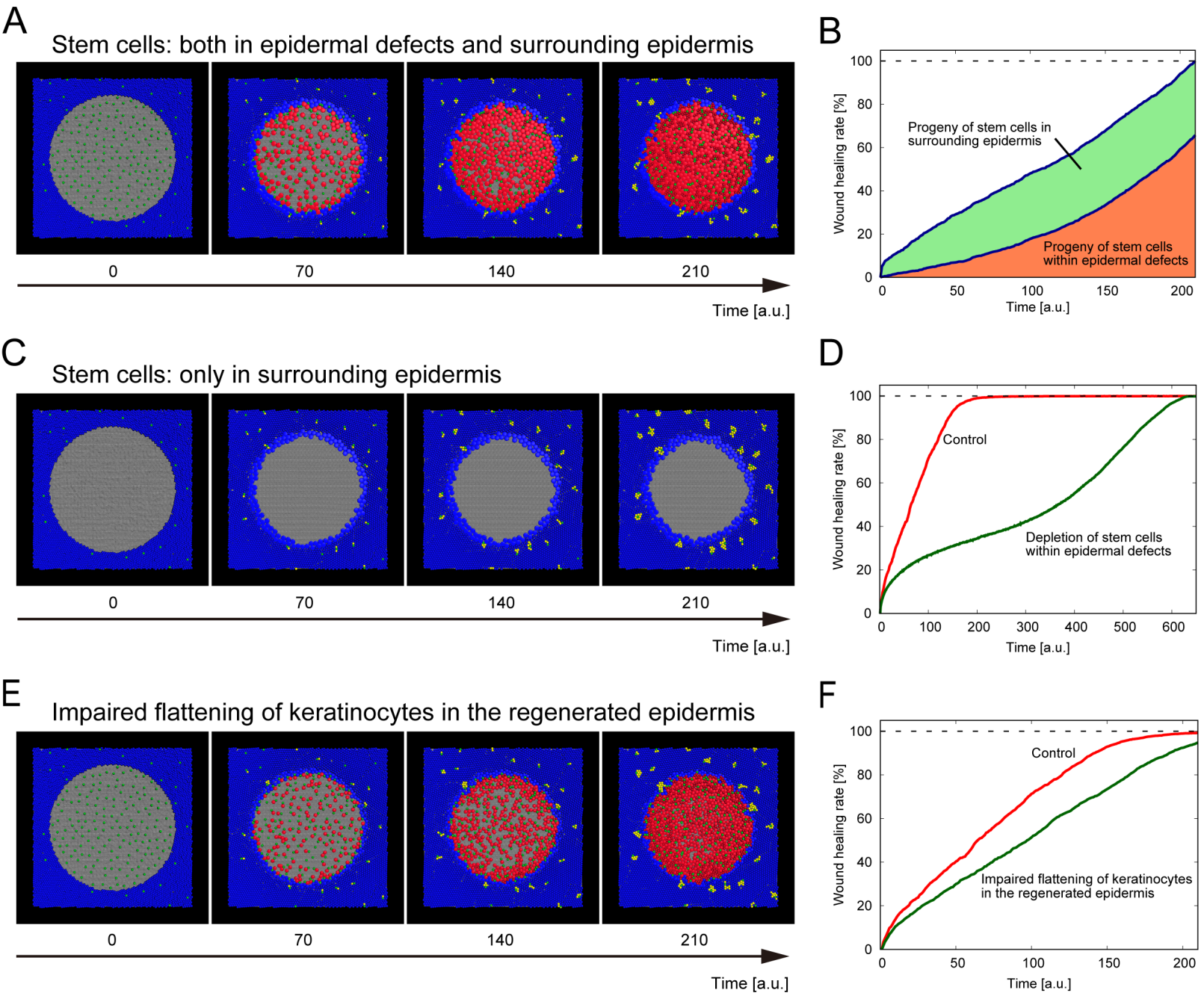

Figure EV1. Healing processes of subepidermal blisters

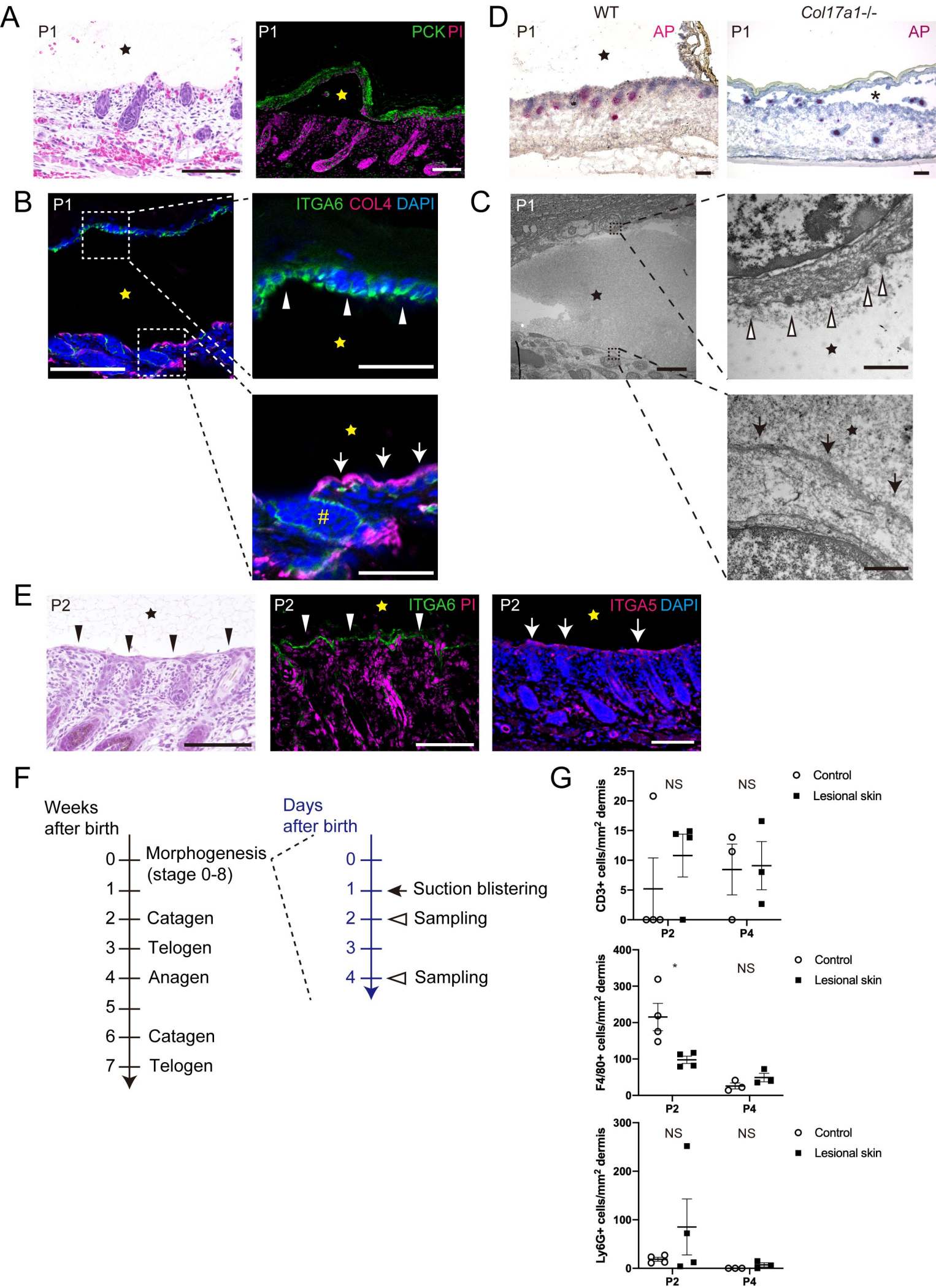

Figure EV2. RNA-seq on blister healing

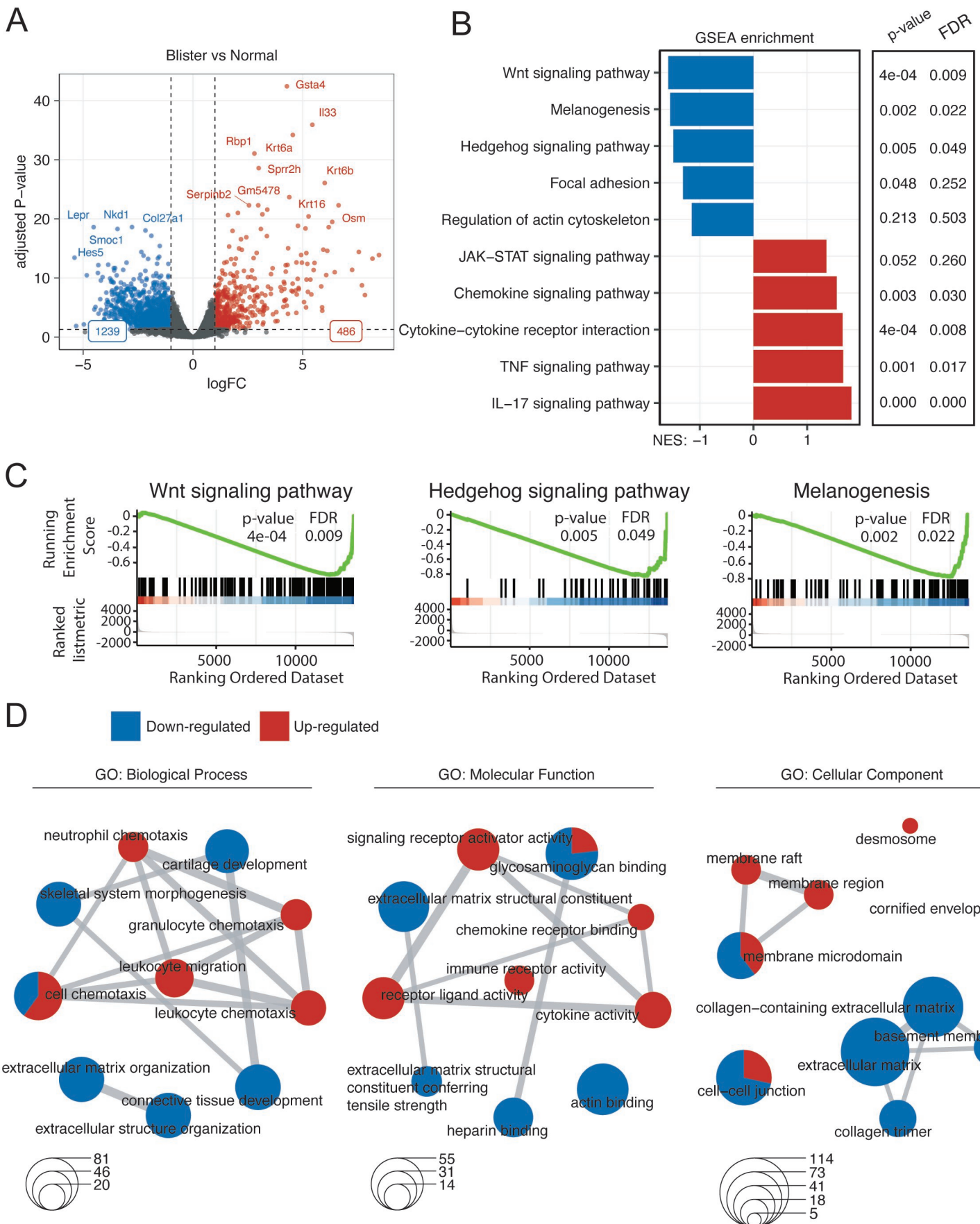

Figure EV3. Lineage tracing of subepidermal blister healing

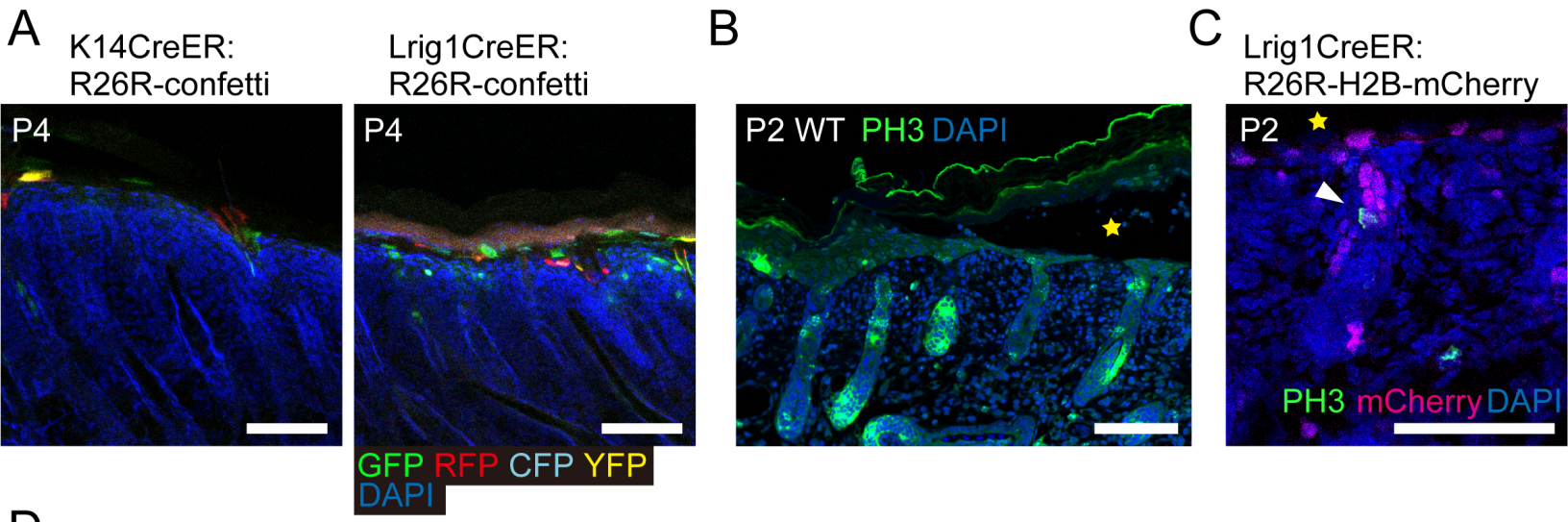

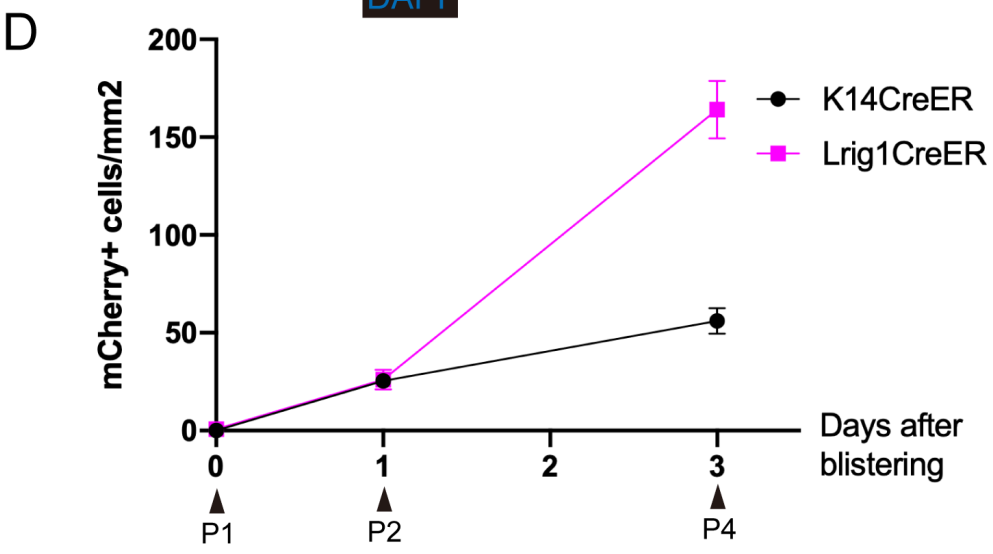

Figure EV4. Dependence of subepidermal blister healing on flattening ratio and SC arrangement

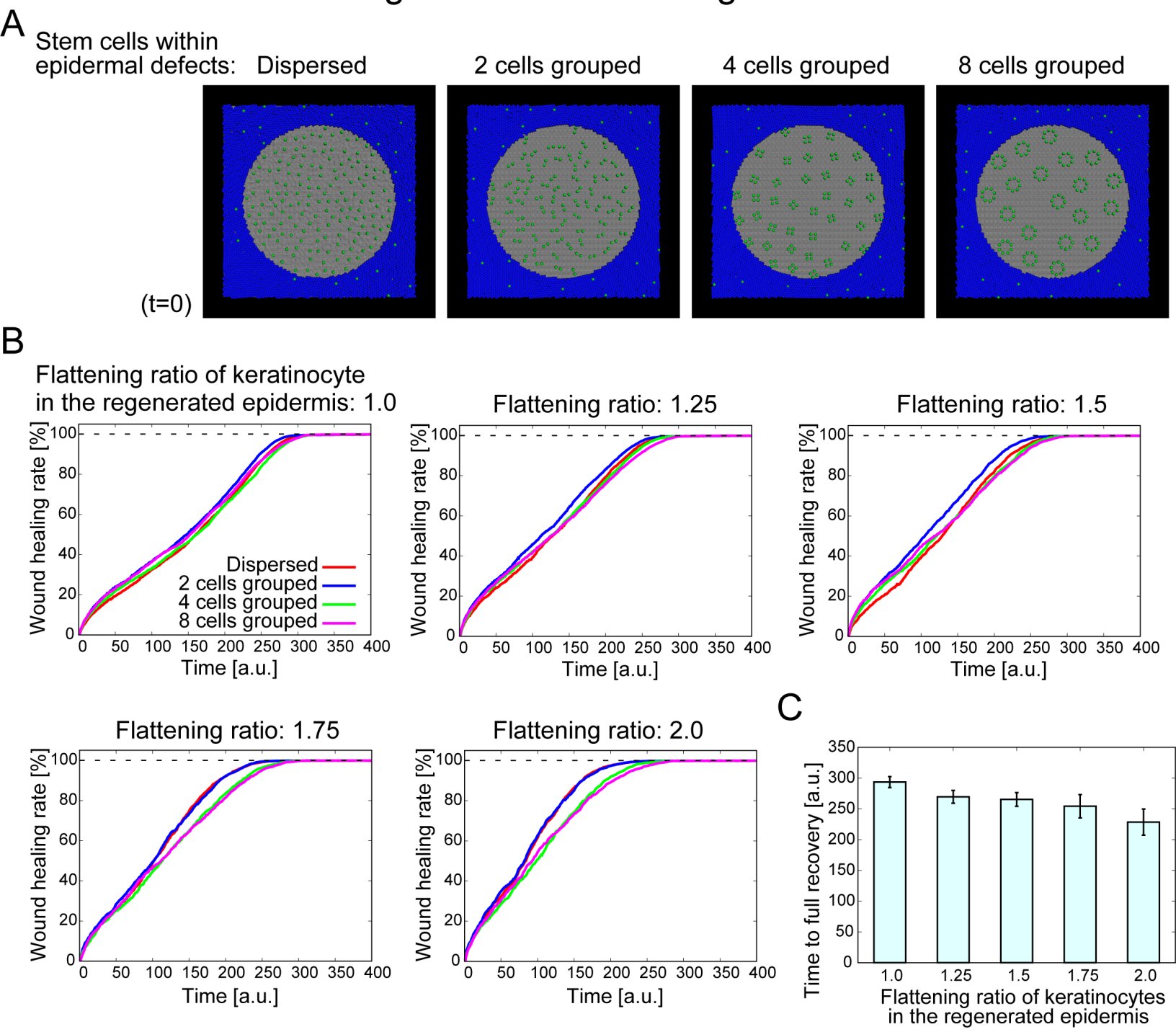

Figure EV5. Subepidermal blister healing in humans